Authors Response for the manuscript: "Remote sensing and modeling analysis of the extreme dust storm hitting Middle East and Eastern Mediterranean in September 2015" by Stavros Solomos et al.

Response to Reviewer #3

General comments

This work is an interesting analysis of a dust storm that was generated over Iraq,Syria and Turkey and then produced a dust plume over the Eastern Mediterranean. The authors approach seems robust and the analysis of the meteorology leading to this dust event is in line with both literature and what I would expect from briefly looking into this particular case. It is generally well written and the figures show what the authors describe. I think more could be made of the conclusion that changes to land surface over relatively short timeframes can be very important for specific dust events (and presumably the overall dust load). Especially with respect to the known interannual variability of particular dust sources such as ephemeral lakes and fluvial deposits from flooding.

We thank the reviewer for the thorough revision and comments. We agree with the importance of time-variant preferential dust sources due to changes in soil properties. The corresponding section has been extended in the revised manuscript and a new plot (Figure 3) has been added to comment on the land-use changes at the area of interest during the previous years. Replies to the specific comments follow below.

Specific comments

45-51 Description of cold pool/haboob production could be made clearer. e.g.
"The responsible mechanism for haboob formation is the generation of a cold pool of ambient air due to evaporative cooling. The rain and ice condensates evaporate (or melt) as they fall through the warmer and unsaturated air and the absorption of latent heat from the phase changes leads in a vigor cooling of the surrounding air.

Haboobs are formed by the evaporation (and melting) of hydrometeors as they fall through warm, unsaturated air below the cloud base of convective clouds. The energy required for these phase changes (latent heat) generates cooled downdrafts. When the downdrafts hit the surface they spread out due to their enhanced density compared with the ambient air. When these The convective outflow boundaries are turbulent and gusty and when they travel over bare soil and desert areas they result in the generation of sediment can be lifted, creating a propagating dust wall."

Done

66 Not all cited works relate to the Atlas mountains remove "as an aftermath of Atlas Mountains convective storms."

Done

125-131 I think section 2.1.3 would benefit from a bit more detail. In particular the production and limitations of the SEVIRI RGB dust images. I would like to direct the authors to the work of Banks & Brindley (2013) (http://dx.doi.org/10.1016/j.rse.2012.07.017) as an evaluation and description of the RGB SEVIRI dust images. Particularly the sensitivity to atmospheric moisture and dust height which is relevant to the interpretation of the SEVIRI dust images when dust is raised at different times and by different processes (recently lifted haboob dust less clearly distinguishable due to high atmospheric water vapour and high stability keeping dust close to the surface). This would be useful to add to the discussion in lines 225-227.

We have updated the corresponding section in the revised manuscript with a more detailed description of the product, and an extended discussion of its possible limitations.

143 I am not familiar with the RAMS model but I suspect the levels are terrain following close to the surface but relax to be smooth and parallel in the upper levels. A little more detail would be useful here.

The vertical coordinate system in RAMS is terrain following sigma-z and the grid stagger is Arakawa C. The first model level is at 50 m above ground and the levels stretch up to about 18 km. We have updated the relevant text accordingly.

157 and figure 1. I think it would be useful to mark on the locations of the radiosonde launch stations on to Figure 1b. Also the frequency of the launches.

Done.

160-162 Did you use any different data for initialisation as part of your sensitivity studies? Roberts et al.(2014) (doi:10.1002/2013JD020667) and Schepanski et al. (2015) doi:10.1002/qj.2453 both show that over West/North Africa the data used for initialisation has a much larger impact on the resultant simulations than other factors such as model resolution, boundary layer set-up or microphysical schemes.

Yes, but we found that our simulations are more sensitive to the location and dimensions of the inner grids rather than to initial conditions. More specifically inclusion of the 2×2 domain was the key to obtain model results that are closer to the observations. It is true that the simulation of the specific event could be further improved, however for the purpose of our study we believe that with the combination of remote sensing and modeling data all the principal processes driving this episode are adequately explained.

196-197 You mention the combination of cold air aloft and low level warming leading to a thermal low. I think it would be better to discuss and even show the 1000-700 hPa thickness and either mean sea level pressure or 925 hpa geopotential height to identify the formation of a thermal low.

Figure 3 is replaced by Figures 4b,c in the revised manuscript. Figure 4b shows the 1000-700 hPa thickness and Figure4c the 925 geopotential height, wind vectors and dust AOD. The corresponding

section has been revised in the manuscript.

238-243 I don't agree with this conclusion borne from Figure 7b that the temperature depression between the rain drops and the ambient air is the "crucial parameter". This is only a single factor that is likely to lead to high evaporation rates and therefore a strong cold pool. Arguably more important is the sub-saturation and depth of the below-cloud air. If below-cloud air is close to saturation and is shallow then regardless of the raindrop-ambient air temperature depression a strong cold pool will not be formed e.g. the patches over Turkey and Syria with similar values but no cold pool. The quantity of water held as hydrometeors is also important. Please amend to make it clear that the situation is more complex.

This is a good point and we agree with the reviewer on the importance of condensate mixing ratio and unsaturated air below the cloud base. The corresponding section has been extended in the revised manuscript, Figure 7a has been revised with the addition of relative humidity and two additional cross-section plots (Figures 7c,d in revised manuscript) have been added to indicate the severity of the particular convective storm. The cross section over the storm reveals the separate updraft-downdraft regions and a rainfall curtain extending from 4-5 km down to the surface. The cloud top is at 12 Km and the generation of a haboob is evident below the non-precipitating parts of the cloud.

251-252 "This latency between satellite and modeled haboob fronts is an indication that the convective downdrafts were in fact stronger." Or could this also be attributed to a triggering delay due to the imperfect modelling of the boundary layer or the stability/moisture profile making conditions for triggering less favourable than in reality. Regardless of cold pool strength these factors could produce later triggering of convection and a latency in the storm progression compared with satellite imagery.

We have rephrased this sentence accordingly: "The latency between satellite and modeled haboob fronts is possibly attributed to a slower propagating modeled haboob or to a triggering delay of convection in the model due to the imperfect representation of boundary layer properties and atmospheric stability."

316-321 It looks like these are thermally driven downslope/upslope winds caused by preferential cooling/heating of the land surface compared to the surrounding sea.

We agree and an extra sentence has been added in the revised text: "Differential heating between the land and water bodies and between flat terrain and mountain slopes results in the development of local wind flows (downslope / upslope winds)."

327-329 There are many factors that could (and likely are) responsible. I think you should include a few more of them here e.g. fall speeds, limitations due to dust emission size bins, transport effects due to imperfect modelling etc.

This sentence is rephrased in the revised manuscript: "(e.g. more intense downward mixing, increased emissions from the sources, limitations due to emission size bins, inaccurate deposition rates etc.)."

Technical corrections
I feel that that work would have benefitted from being proof read by someone who is a native English speaker. There are occasions when slight errors disrupt the flow of the text. I have highlighted errors that I have seen below.

We appreciate the thorough language review and we have corrected the text accordingly.

For example.
42-43 "These systems are well known by local populations at in desert and arid areas worldwide due to their devastating impact in on human health"
Done.

64 "A variety of studies on haboobs has have been performed worldwide."
Done.

Make sure acronyms are always defined where they first appear in the text. For example.
55 "SAMUM 1 & 2" is not defined. SAharan Mineral dUst experiMent.
Done.

56 "MODIS"
Done.

105 "CALIOP" CALIPSO is defined but not CALIOP
Done.

Use "led" not "lead" throughout e.g. 66 and 89.
Done.

Wherever UTC time is used it would be useful for interpretation to include local time (LT) in brackets afterwards.

The experimental domain is quite extended and includes several time zones. We prefer to use UTC throughout the text for consistency.

Be consistent with use of AOD or AOT, they are interchangeable.

Done (AOT is used throughout the revised text).

53 "Moreover, haboobs are usually generated over remote ..."
58 "It is also worth to mentioning..."
71 "synergy" I don't really like this term here. I'm not sure the effect is greater than the sum of the individual parts. If you are talking about specific positive feedbacks

then be specific. If not you can just remove "and synergy"
114 "km analysis and vertical resolution..."
144 "dust production emission scheme"
187-188 "the combination between of two distinct meteorological features in the greater area:"
202 "extended bare soil areas in Syria (Figure 2)."
213 "As seen in Figure 4, shows the convergence..."
221 "(plume_2) also was detected..."
223 "the approach approaching of the..."
233-234 "circulation and as is shown in Figure 6b. it It is characterized..."
234 "Somalia"
259 "Figures 8 9 and 9 10"
272 "bellow"
281 "observations again suffers again from total..."
296 "Libanon Lebanon"
367 "regarding the forecast skills of the atmospheric..."
368 "such extreme episodes are very seldom, they still..."
370 "atmosphere are nowadays now often adequately..."

All spelling and grammar corrections are applied to the revised manuscript.

374 "systems for dust episodes in West Africa."

We have rephrased the sentence : "Moreover, a recent study by Pope et al. (2016) at the area of Sahel/southern Sahara suggests that unresolved haboobs during the summer monsoon may be responsible for up to 30% of the total atmospheric dust and such considerations raise questions on the current status of early warning systems for dust episodes."

375 "the complexity of these events makes their forecast forecasting them very ..."

Done

Figures

Figure 1a Change the scale used here. I don't understand why you would only use the lowest third of the values specified on a colourbar. Label countries (at least Syria, Turkey and Iraq) for ease of interpretation.

Done (Figure 4a in revised manuscript).

Figure1b Include location of radiosondes that are assimilated. Their influence is obviously limited to a certain distance and time from the launch so knowing their position and frequency is important.

Done (Figure 1 in revised manuscript).

Figures 3, 5, 8, 9 & 10. Where possible SEVIRI RGB images should be cropped closer to the model domain they are compared with, either this or show more of the region and draw the domain box on top of the satellite imagery (Figure 5 was especially difficult to interpret) as the different panels are zoomed in different amounts and the model domains are rotated compared with the satellite imagery.

As the reviewer also states the different projection between satellite and model images makes their intercomparison somehow tricky. We revised the aforementioned figures including indication of the model domain over the corresponding satellite images whenever possible.

Figure 4. I think that it would be better for interpretation if the style and parameters plotted were changed slightly. Currently topography over 900 m is shaded. In reality we don't need this detail. You also discuss convergence but do not calculate or show it and interpreting convergence from wind vectors is very difficult. I suggest that you keep the vectors and the red contours for cloud (maybe make the contour lines thicker), but change the topography contours to a single blue or green contour at 1000 m. Then use colour filled contours (or greyscale) to show convergence. This can be as simple as a centred finite difference approach to show where the important convergence zones are.

We have revisited this plot based on the reviewer's suggestions. Indeed no convergence zones are found. Moreover, the near surface wind field does not contribute to the transport of dust which occurs at levels above 1 km along with the convective outflow from the mountains of Turkey. Figure 4 is removed from the revised manuscript.

Figure 6b Mark on location of domain shown in 6a.

Done

Figure 7 As discussed in Specific comments I do not agree that the rain droplet to air temperature difference is the crucial parameter in the formation of the cold pool shown. Change 7a to be of colour contours of boundary layer sub-saturation or dew-point depression and have line contours of the rain droplet –air temperature difference overlaid on top. This would show where the sub-

saturation was strongest as well as where the temperature difference is greatest and where there are hydrometeors present.

Figure 7a has been revised following the reviewer's recommendations and two cross-section plots (Figures 7c,d) have been added to illustrate the severity of the convective storm and the generation of a density current haboob.

Figures 9 and 10 should have an additional panel added that shows the model dust load marked with the cross section (equivalent to 9a and 10a). This would help with interpretation, especially given the delay in triggering of convection discussed in the paper.

Done

Response to reviewer #4

We thank the reviewer for the comments and suggestions. All corrections are taken into consideration in the revised manuscript.

Response to short comment

Thanks for your comment. The following sentences have been added at the conclusions section in the revised manuscript: "The key for forecasting these events in atmospheric models is the use of cloud resolving grid space. Forthcoming studies using an extended high-resolution grid over the entire Middle-East (e.g. Gasch et al., 2017) could provide more detail on the specific atmospheric processes during this episode".
The highest AOD values in the simulations are at the range 10-15. Extreme values > 20 are found over a few model grid points over the sources and due to the accumulation and overlapping of multiple dust layers. Such values are probably unrealistic; however the specific episode has indeed extraordinary characteristics.

List of changes

Line 21: and,
Line 22: as well as
Line 24: of modeling and remote sensing data
Line 28: Northern
Line 29: westward moving haboobs that merge
Line 30: Northern
Line 38: in this…… the Eastern
Line 39: Northern
Line 44: in desert
Line 45: on visibility
Lines 46-56: Haboobs are formed by the evaporation (and melting) of hydrometeors as they fall through warm, unsaturated air below the cloud base of convective clouds. The energy required for these phase changes (latent heat) generates cooled downdrafts. When the downdrafts hit the surface they spread out due to their enhanced density compared with the ambient air. These convective outflow boundaries are turbulent and gusty and when they travel over bare soil and desert areas sediment can be lifted, creating a propagating dust wall.
Line 59: haboobs are
Line 60: generated…….. in-site
Line 61-62: (e.g. SAharan Mineral dUst experiment (SAMUM)
Line 64-65: (e.g. Moderate Resolution Imaging Spectroradiometer (MODIS),
Line 66: Thickness (AOT),
Line 70: AOT
Line 72: have been…… For example
Line 74: that lead in severe haboob formation in Sahara.
Line 79: of the
Line 89: presented
Line 91: Therefore
Line 92: over Cyprus
Line 99: led
Line 106-108: The EARLINET lidar network is widely used for aerosol characterization and particularly for dust characterization studies (Mona et al., 2012).
Lines 110-112: For this case study we use a lidar ratio of 40 sr that is typical for Middle East dust (Mamouri et al., 2013). The overall uncertainty in the estimated dust mass concentrations is 20-30%.

Line 116: The Cloud-Aerosol Lidar with Orthogonal Polarization (CALIOP),
Line 123-124: The CALIPSO algorithms are described in detail by Winker et al. (2009).
Line 125: resolution of 5 km and vertical
Lines 135-137: For this case study we use a lidar ratio of 40 sr that is typical for Middle East dust (Mamouri et al., 2013). The overall uncertainty in the estimated dust mass concentrations is 20-30%.

Line 140: a combination of three infrared
Line 141: channels of SEVIRI

Lines 142-160: The channel combination and visualization parameters (Table 1) were chosen to maximize the visual contrast between the hot desert surface and lofted dust particles (Lensky and Rosenfeld, 2008). During daytime, the hot desert sand, made up from large quartz particles, appears white/blue due to the large difference in emissivity of IR10.8 and IR8.7 channels (green), high temperature (blue), and quite large difference in IR12.0 and IR10.8 channels (red). In contrast, lofted dust plumes with fine quartz particles have similar values of emissivity at IR10.8 and IR8.7 and this makes dust appear pink or magenta. Deep cumulonimbus clouds are depicted with red colors, while thick water clouds appear yellow. The RGB dust product is a very useful tool to qualitatively monitor dust transport events, taking advantage of the high temporal resolution of SEVIRI observations. The dust RGB product is provided in hourly intervals by EUMETSAT (European Organization for the Exploitation of Meteorological Satellites) and is used in this work to monitor the evolution of the dust transport event. In some cases, however, the usefulness of the product can be limited and this should be considered in the following discussion. First, the visual contrast of dust and the underlying surface is diminished when the temperature difference of the two is low, e.g. during nighttime. Second, high levels of columnar water vapor or the presence of the temperature inversion can mask the presence of dust in the atmosphere (Brindley et al., 2012). Finally, the contrast of dust and the ground can be further diminished over some type of surfaces e.g. over rocky terrain, due to its high emissivity at the 8.7 μm channel (Banks and Brindley, 2013).

Line 175: 50 sigma-z terrain

Line 176: The first model level is at 50 m above ground and the levels stretch from

Line 177: The dust emission scheme

Line 191: , 00Z and 12Z), ……., 00Z and 12Z

Line 192: , 00Z and 12Z……, 21Z……, 00Z

Line 199-200: hampered by seasonal and interannual variability of dust sources together with recent

Lines 202-204:Firstly, this annual-mean dataset cannot accurately describe the land use and dust sources at the end of the dry season in the Middle East., Secondly, the

Line 206: led to further changes

Line 208: between August

Lines 211- 224: The impact of the ongoing conflict on land use and vegetation can be further highlighted in Figure 3, showing the time series of MODIS NDVI in the region around Hawija, Kirkuk province, Iraq (region B of Fig.2). Agriculture in Hawija is based on a combination of rain-fed and

irrigated fields, in accordance with a rainy and a dry season from November to May and from June to October respectively. The NDVI time series clearly captures this behavior, with a major annual NDVI pick during wet months and a smaller cycle during each summer, probably reflecting the growth of summer crops with the help of irrigation. This summer cycle is completely absent in 2015. Indeed, a recent survey of the Food and Agriculture Organization (FAO) of the United Nations, reveals that large parts of the irrigation system in Kirkuk and surrounding regions have been destroyed by military operations and a large number of pumps and generators required for irrigation have been stolen (Singh N. et al, 2016). This, together with the destruction of other agricultural equipment and infrastructures, has severely disrupted the summer agriculture activities of 2015, exactly before the dust storm studied here, leaving the fields to act as very efficient dust sources.

Line 236-237: combination of two

Line 245-246: Advection of warm air from the Red Sea is also evident at the lowest troposphere by the 1000-700 mb thickness in Figure 4a.

Line 248: Syria that is evident by the 925 mb geopotential height in Figure 4b.

Line 255-258: and result in the mobilization of dust in the area. Dust uptake is mostly evident at the outer parts of the cyclone where surface wind speed exceeds

Line 262: Figure 4b

Line 263: Figure 4c

Lines 264-266: The convective outflows from the Zagros Mountains in Turkey that are evident by the black dashed line and wind vectors at 925 mb in Figure 3b enhance the mobilization of dust at the northern parts of the heat low.

Line 270: Cyprus is evident

Line 273: Mamouri et al.(2016). The faster propagating haboob plume (plume_2)

Line 276: In the model, approach of the haboob

Line 279: over Northern Syria and Southern Turkey

Line 283: on 6 September

Line 286: circulation and is

Line 287: Figure 6b. It is characterized by strong SW winds blowing from the Somali

Line 290-291: Low-level advection of warm towards the storm area also evident in Figure 6c by the 1000-700 mb modeled thickness at 15:00 UTC.

Line 293: A number of atmospheric parameters that determine the formation of the cold

Line 294: are shown in Figures7a-d.

Line 295: iso-temperature line of -20°C between

Line 297-299: clearly defines the cold pool area. Sub-saturated air below the cloud base is also evident in Figure 7a since the relative humidity at the neighbor of the convective cloud is between 15-20 %. The combination of sub-saturated air and

Line 300-301: and in the formation of a cold pool at the area of Northern Iraq with speeds ranging from

Line 302-308: The convective cloud top reaches 12 km and the updrafts exceed 18 m s^{-1} at 15:00 UTC (Figure 7c). The rainfall curtain (downdraft area in Figure 7c) extends up to 4-5 km and the severity of the storm leads in the formation of a haboob that is evident by the streamline structure and dust production below the non-precipitating parts of the cloud in Figure 7d. A Kelvin-Helmholtz billow at 2-3 km separates the density current head from the ambient flow similar to previous findings for convective haboobs (Solomos et al., 2012). Dust particles are distributed inside the system and dust concentrations exceed 2000 μg m^{-3} below the cloud. As the cold

Line 313: surface modelled

Lines 315-318: The latency between satellite and modeled haboob fronts is possibly attributed to a slower propagating modeled haboob or to a triggering delay of convection in the model due to the imperfect representation of boundary layer properties and atmospheric stability.

Line 326: Figures 9 and 10. All heights in satellite and model profiles refer to heights above surface

Line 328-329: The modeled dustload is also shown in Figure 9b for comparison. Dust concentrations are estimated from CALIPSO lidar signal

Line 330: Figure 9c they

Line 332: model (Figure 9d).

Line 340: totally attenuated below ~1 km

Line 342: at this area in the top 500m of the propagated haboob (1-1.5 km),

Line 345: The modeled dustload is also shown in Figure 10b for comparison

Line 348: (Figure 10c)

Line 350: observation again suffers

Line 352: from CALIPSO at the edge

Line 358: west of the CALIPSO ground track

Line 363: the lidar on 7 September

Line 365: off the coast of Lebanon

Line 373: On 8

Line 378: on 8 September

Line 383: during 8 September

Line 385-387: Differential heating between the land and water bodies and between flat terrain and mountain slopes results in the development of local wind flows (downslope / upslope winds).

Line 398: mixing, increased

Line 399: sources, limitations due to emission size bins, inaccurate deposition rates etc.).

Line 400: Table 2.

Line 416: Middle East and the Eastern

Line 422: of strong thermal low and convective outflows

Line 424: of moist and unstable air masses from the Arabian Sea and the Red Sea

Line 439: forecast skill

Line 440: are seldom, they

Line 442: are now often adequately

Line 444: Pope et al. (2016) at the area of Sahel/southern Sahara suggests

Line 445: haboobs during the summer monsoon

Line 448: makes forecasting them

Lines 449-458: As shown at the present study, the complexity of these events makes forecasting them very challenging and it is possible that a certain model configuration could successfully reproduce a specific event but not all similar events. The key for forecasting these events in atmospheric models is the use of cloud resolving grid space. However, such high resolution grid-space can only be applied over limited areas due to restrictions in computational power. Forthcoming studies using an extended cloud-resolving grid over the entire Middle-East (e.g. Gasch et al., 2017) could provide more detail on the individual atmospheric processes during this episode.

Line 465: activation of correlated

Line 496: Banks, J. R. and Brindley, H. E.: Evaluation of MSG-SEVIRI mineral dust retrieval products over North Africa and the Middle East, Remote Sensing of Environment, 128, 58–73, doi:10.1016/j.rse.2012.07.017, 2013.

Line 508: Brindley, H., Knippertz, P., Ryder, C. and Ashpole, I.: A critical evaluation of the ability of the Spinning Enhanced Visible and Infrared Imager (SEVIRI) thermal infrared red-green-blue rendering to identify dust

events: Theoretical analysis, J. Geophys. Res., 117(D7), D07201, doi:10.1029/2011JD017326, 2012.

Line 528: Gasch, P., Rieger, D., Walter, C., Khain, P., Levi, Y., and Vogel, B.: An analysis of the September 2015 severe dust event in the Eastern Mediterranean, Atmos. Chem. Phys. Discuss., doi:10.5194/acp-2017-11, in review, 2017.

Line 571: Mona L., Z. Liu, D. Müller, A. Omar, A. Papayannis, G. Pappalardo, N. Sugimoto and M. Vaughan, "Lidar Measurements for Desert Dust Characterization: An Overview," Advances in Meteorology, vol. 2012, Article ID 356265, 36 pages, 2012. doi:10.1155/2012/356265

Line 606: Singh N., van Zoonen D., and Khogir M.: Iraq agriculture and livelihoods needs assessment in the newly liberated areas of Kirkuk, Ninewa and Salahadin, Food and Agricutlure Organization of the United Nations, 2016.

Lines 644-649 : Table 1 …… Table 2

Line 656: Revised Figure 1.

Line 659: and black stars the location of radiosondes.

Line 678: New Figure 3.

Line 687: Revised Figure 4.

Line 687: a) Model 1000-700 mb thickness (dam), 6 September 2015, 00:00 UTC. Model AOT

Line 694: Remove old Figure 4

Line 705: Revised Figure 5

Line 706-707: The white rectangular approximately indicates the location of the model domain shown in Figure 5a.

Line 718: Revised Figure 6

Line 719: Wind speed at 975 mb

Lines 720-721: The white rectangular indicates the location of the model domain shown in Figure 6a.

c) Model 1000-700 mb thickness (dam), 6 September 2015, 15:00 UTC

Line 730: Revised Figure 7.

Lines 730-737: Figure 7. a) Model relative humidity at the first model level (color scale) and -20°C iso-temperature line (red contours) of rain droplets air temperature difference. b) Model wind speed at 10m (ms^{-1}). The dashed line denotes the location of the cold pool and the solid black line the location of the storm cross-sections of Figures 7c,d c) Vertical cross section of total condensate mixing ratio (blue contours in g k g^{-1}) and vertical wind component (vectors and color scale in m s^{-1}). The dashed line separates updraft (positive w) from downdraft/precipitating regions (negative w). d) Vertical cross section of total condensate mixing ratio (blue contours in g k g^{-1}), dust concentration (μg m^{-3}) and flow streamlines, 6 September 2015, 15:00 UTC

Line 741: Revised Figure 8

Lines 743-744: front location and the dashed rectangular in Figure 8c approximately indicates the location of the model domains shown in Figures 8a,b.

Line 751: Revised Figure 9.
Line 751: Model dustload (mg m^{-2}) c)
Line 752: (µg m^{-3}) and d) model dust
Line 764: b) Model dustload (mg m^{-2}) c)

Revised (marked-up manuscript version) with track changes

Remote sensing and modeling analysis of the extreme dust storm hitting Middle East and Eastern Mediterranean in September 2015

Solomos Stavros[1], Albert Ansmann[2], Rodanthi-Elisavet Mamouri[3], Ioannis Binietoglou[1,5], Platon Patlakas[4], Eleni Marinou[1,6] and Vassilis Amiridis[1]

[1]Institute for Astronomy, Astrophysics, Space Applications and Remote Sensing (IAASARS), National Observatory of Athens, Athens, Greece
[2]Leibniz Institute for Tropospheric Research, Leipzig, Germany
[3]Cyprus University of Technology, Department of Civil Engineering and Geomatics, Limassol, Cyprus
[4]School of Physics, Division of Environment and Meteorology, University of Athens, Athens, Greece
[5]National Institute of R&D for Optoelectronics, Magurele, Ilfov, Romania
[6]Laboratory of Atmospheric Physics, Physics Department, Aristotle University of Thessaloniki, 54124, Thessaloniki, Greece

Abstract The extreme dust storm that affected Middle East and the Eastern Mediterranean in September 2015 resulted in record-breaking dust loads over Cyprus with aerosol optical depth exceeding 5.0 at 550 nm. We analyze this event using profiles from the European Aerosol Research Lidar Network (EARLINET) and~~,~~ the Cloud-Aerosol Lidar and Infrared Pathfinder Satellite Observation (CALIPSO) as well as~~,~~ geostationary observations from the *Meteosat Second Generation* - Spinning Enhanced Visible and Infrared Imager (MSG-SEVIRI) and high resolution simulations with the Regional Atmospheric Modeling System (RAMS). The analysis of modeling and remote sensing data reveals the main mechanisms that resulted in the generation and persistence of the dust cloud over Middle-East and Cyprus. A combination of meteorological and surface processes is found: (a) the development of a thermal low at the area of Syria that results in unstable atmospheric conditions and dust mobilization at this area; (b) the convective activity over Northern Iraq that triggers the formation of ~~a~~ westward moving haboobs that merge~~s~~ with the previously elevated dust layer; and (c) the changes in land use due to war at the areas of Northern Iraq and Syria that enhances dust erodibility.

1. Introduction

A record dust storm affected the entire Middle East and Cyprus in September 2015. Remote sensing observations and in-situ measurements of Arabian dust from this episode during 7-11 September 2015 are presented by Mamouri et al. (2016) for the station of Limassol (34.7°N, 33°E). As reported in ~~their~~ this article, the extreme amounts of dust over Middle East and the Eastern Mediterranean originate from the desert and arid areas of Syria and Northern Iraq. Triggered by this work, we analyze here the main processes that resulted in the mobilization of dust due to a combination of cyclonic flow and haboob formation.

Haboobs are local and mesoscale atmospheric density currents that mobilize huge amounts of dust and create a propagating dust wall extending up to 2-3 km in the troposphere (Knippertz et al., 2009; Solomos et al., 2012). These systems are well known by local populations ~~at~~ in desert and arid areas worldwide due to their devastating impact ~~in~~ on visibility and human health (e.g. Schepanski et al., 2009; Emmel et al., 2010). ~~The responsible mechanism for haboob formation is the generation of a cold pool of ambient air due to evaporative cooling. The rain and ice condensates evaporate (or melt) as they fall through the warmer and unsaturated air and the absorption of latent heat from the phase changes leads in a vigor cooling of the surrounding air. When these convective outflow boundaries travel over bare soil and desert areas they result in the generation of a propagating dust wall.~~ Haboobs are formed by the evaporation (and melting) of hydrometeors as they fall through warm, unsaturated air below the cloud base of convective clouds. The energy required for these phase changes (latent heat) generates cooled downdrafts. When the downdrafts hit the surface they spread out due to their enhanced density compared with the ambient air. These convective outflow boundaries are turbulent and gusty and when they travel over bare soil and desert areas sediment can be lifted, creating a propagating dust wall. The scale of the processes that participate in the generation of such atmospheric density currents ranges from synoptic down to mesoscale and local. As a result, haboobs and their effects in weather and air-quality cannot be resolved by the coarse global model resolutions (Marsham et al., 2013). Moreover, haboobs are usually generated over remote arid areas where no in-situ networks are present and ~~inside~~ in-site dust-storm measurements can only be obtained during field campaign experiments (e.g. SAharan Mineral dUst experiment (SAMUM) 1 & 2, Ansmann et al., 2011; FENNEC, Ryder et al., 2015). Following these limitations, most of the efforts for the studying and forecasting of such intense dust episodes rely on passive and active

remote sensing observations (e.g. Moderate Resolution Imaging Spectroradiometer (MODIS), EARLINET, CALIPSO) and on high resolution modeling simulations. Assimilation of satellite derived Aerosol Optical ~~Depth~~ Thickness (AOT~~D~~), has been shown to improve the dust forecasts in global models especially for the long range transport (Benedetti, et al., 2009); however this approach cannot be easily adopted for the description of haboobs. The reason is that the convective events and the associated wind gusts are not properly resolved at coarse model resolutions. As a result, assimilating the satellite ~~AOD~~ AOT over an inaccurate meteorological field does not improve the dust forecast.

A variety of studies on haboobs ~~has~~ have been performed worldwide. For example Knippertz et al. (2009); Reinfried et al. (2009); Solomos et al. (2012); Roberts and Knippertz (2014)~~,~~ analyzed the physical processes that lead in severe haboob formation in Sahara ~~as an aftermath of Atlas Mountains convective storms~~. Bou Karam et al. (2008) showed the contribution of the east Atlantic monsoon flow and the associated mesoscale convective systems (MCS) in dust elevation along the Sahel. Vukovic et al. (2014) described the severe convective dust storm that hit Phoenix Arizona in July 2011. Asian haboobs from the Taklimakan and Gobi deserts are described and simulated in Takemi~~,~~ (1999, 2005). All these studies agree in the complexity ~~and synergy between~~ of the various physical processes at multiple atmospheric scales that govern the generation and lifetime of these systems. Apart from their devastating effects at local and near surface scales, such events may also contribute to the free-troposphere dust burden in several ways: First, entrainment of dust particles in the free troposphere takes place at the turbulent region of the density current head (Takemi, 2005; Solomos et al., 2012); Second, they trigger secondary convective cells along their pathways that may evolve to synoptic scale dust events and third, dust residuals remain aloft after the cold pool declines.

The current article is the second part (Part 2) in a series of articles on the September 2015 extraordinary dust storm in Middle East and Eastern Mediterranean. In Part 1, Mamouri et al. (2016) presented a detailed analysis of remote sensing and in-situ monitoring of the event over Cyprus. The formation of similar events is not fully understood and we use this unique episode to elucidate the mechanism of dust production in this understudied region. Therefore EARLINET measurements over Cyprus along with CALIPSO and MSG observations are used to fine tune RAMS simulations and explain the physical processes that resulted in this haboob-driven dust storm. We focus our analysis on the first two days of the event (6 and 7 September 2015) when the extraordinary dust-storm was generated. To the best of our knowledge this is the first detailed modeling and remote sensing study to describe a Middle East haboob. The modeling and measurement techniques for the analysis are

presented in Section 2. Section 3 includes the model results, the remote sensing observations and the investigation of the atmospheric processes that ~~lead~~ led in the formation of the dust episode. Conclusive remarks and discussion are presented in Section 4.

2. Instruments and models.

2.1 Remote sensing observations

2.1.1. EARLINET

The lidar station at Limassol (34.7° N, 33° E; 23 m above sea level, a.s.l.) is part of the European Aerosol Research Lidar Network (EARLINET: Pappalardo et al., 2014). The EARLINET lidar network is widely used for aerosol characterization and particularly for dust characterization studies (Mona et al., 2012). Details on the lidar station equipment and the retrieval algorithms are given in Mamouri et al. (2016). Dust mass concentration profiles are obtained from the dust optical properties following the methodology proposed by Ansmann et al. (2012). For this case study we use a lidar ratio of 40 sr that is typical for Middle East dust (Mamouri et al., 2013). The overall uncertainty in the estimated dust mass concentrations is 20-30%.

2.1.2. CALIPSO

The Cloud-Aerosol Lidar with Orthogonal Polarization (CALIOP), the principal instrument on board the CALIPSO satellite is a standard dual-wavelength (532 and 1064 nm) backscatter lidar, operating a polarization channel at 532 nm (Winker et al., 2009). CALIOP has been acquiring high-resolution profiles of the attenuated backscatter at 532 and 1064 nm along with polarized backscatter in the visible channel since 2006. After calibration and range correction of the lidar backscatter signals (Level 1 CALIPSO product), cloud and aerosol layers are identified and aerosol backscatter and extinction coefficient profiles at 532 and 1064 nm are retrieved as part of the Level 2 CALIPSO product. The CALIPSO algorithms are described in detail ~~in a special issue of the Journal of Atmospheric and Oceanic Technology (e.g.,~~ by Winker et al.~~,~~ (2009). In this study, we utilize L2 version 3 Aerosol and Cloud profiles product at a horizontal resolution of 5 km ~~analysis~~ and vertical resolution of 60 m (in altitudes up to 8 km above sea level). In extreme haboob events, where the optical signal is very high, it is possible for the algorithm to wrongly attribute a dust layer as a cloud. In order to address this issue and fully understand the observed scene we use collocated information derived from MSG-

SEVIRI (see sect. 2.1.3). In the two CALIPSO cases used here, MSG-SEVIRI RGB images confirmed that CALIPSO overpasses was cloud free, hence we classify both aerosol and cloud categorized CALIPSO observations as aerosol.

Moreover, both of the cases have significantly high particle depolarization ratio values, which is a signature of pure dust scenes. In order convert the dust extinction coefficient from CALIPSO into dust mass concentration, we follow the methodology proposed by Ansmann et al. (2012) using the conversion parameter of desert dust that is proposed in Mamouri and Ansmann (2017). For this case study we use a lidar ratio of 40 sr that is typical for Middle East dust (Mamouri et al., 2013). The overall uncertainty in the estimated dust mass concentrations is 20-30%.

2.1.3. MSG-SEVIRI

The Meteosat dust RGB composite is produced from a combination ~~between~~ of three ~~MSG~~infrared channels of SEVIRI: IR12.0-IR10.8 (red), IR10.8-IR8.7 (green), and IR10.8 (blue). The channel combination and visualization parameters (Table~~.~~ 1) were chosen to maximize the visual contrast between the hot desert surface and lofted dust particles (Lensky and Rosenfeld, 2008). During daytime, the hot desert sand, made up from large quartz particles, appears white/blue due to the large difference in emissivity of IR10.8 and IR8.7 channels (green), high temperature (blue), and quite large difference in IR12.0 and IR10.8 channels (red). In contrast, lofted dust plumes with fine quartz particles have similar values of emissivity at IR10.8 and IR8.7 and this makes dust appear pink or magenta. Deep cumulonimbus clouds are depicted with red colors, while thick water clouds appear yellow. The RGB dust product is a very useful tool to qualitatively monitor dust transport events, taking advantage of the high temporal resolution of SEVIRI observations. The dust RGB product is provided in hourly intervals by EUMETSAT (European Organization for the Exploitation of Meteorological Satellites) and is used in this work to monitor the evolution of the dust transport event.

In some cases, however, the usefulness of the product can be limited and this should be considered in the following discussion. First, the visual contrast of dust and the underlying surface is diminished when the temperature difference of the two is low, e.g. during nighttime. Second, high levels of columnar water vapor or the presence of the temperature inversion can mask the presence of dust in the atmosphere (Brindley et al., 2012). Finally, the contrast of dust and the ground can be further diminished over some type of surfaces e.g. over rocky terrain, due to its high emissivity at the 8.7 μm

channel (Banks and Brindley, 2013). ~~This product is provided in hourly intervals by EUMETSAT (European Organisation for the Exploitation of Meteorological Satellites) and aims in the monitoring of dust transport. Dust in these RGB images appears in pink or magenta colors while green-blue and red-brown colors are reserved for land and clouds respectively (Lensky and Rosenfeld, 2008).~~

2.2 Modeling simulations

2.2.1 RAMS-ICLAMS model

For the simulations used in this study we adopt the online coupled atmospheric and air quality modeling system RAMS-ICLAMS (Pielke et al., 1992; Meyers et al., 1997; Cotton et al., 2003; Solomos et al., 2011). The Integrated Community Limited Area Modeling System (ICLAMS) is an enhanced version of RAMS6.0 and it has been developed by the Atmospheric Modeling and Weather Forecasting Group at the University of Athens, Greece. The model is set up in a two-way nesting configuration. The external domain grid space is set at 12×12 km and the grid space of the inner domain is set at 4×4 km. A higher resolution (cloud resolving) grid at 2×2 km is nested over the haboob generation area at Syria-Iraq-Iran-Turkey borders. The locations of the model domains are shown in Figure 1b. The vertical structure of the model consists of 50 sigma-z terrain following levels. The first model level is at 50 m above ground and the levels stretch~~ing~~ from the surface up to 18 km. The dust ~~production~~ emission scheme follows the saltation and bombardment approach (Marticorena and Bergametti 1995; Spyrou et al., 2010). Wet and dry deposition of dust is formulated following Seinfeld and Pandis 1998. Mineral dust is represented with a transport mode of eight radii bins namely 0.15, 0.25, 0.45, 0.78, 1.3, 2.2, 3.8 and 7.1 μm. Sea salt aerosol is also parameterized following Monahan et al., 1986; Zhang et al., 2005; Leeuw et al., 2000 and Gong et al., 2002, 2003 and it is represented with an accumulated and a coarse mode at 0.18 μm and 1.425 μm in radius respectively. Dust and sea salt particles interact with the radiative transfer code of the model (Rapid Radiative Transfer Model (RRTM), Mlawer et al., 1997; Iacono et al., 2000) for the computation of heating rate fluxes. The formation of cloud condensation nuclei (CCN) and ice nuclei (IN) from dust and sea salt particles is also included in the model based on the schemes of Fountoukis and Nenes, 2005 and Barahona and Nenes 2009. Initial and boundary conditions are from the NCEP final analysis dataset (FNL at 1°×1° resolution) and the sea surface temperature is the NCEP operational SST at 0.5°×0.5°. The convective parameterization scheme of Kain and Fritsch, 1993 (KF) is activated for the two coarser grids. Assimilation of radiosonde data from the airports of Adana (36.98°N, 35.35°E, 00Z and

12Z), Bet Dagan (32.00°N, 34.81°E, 00Z and 12Z), Diyarbakir (37.54°N, 40.12°E, 00Z and 12Z), Mafraq (32.36°N, 36.25°E, 21Z) and Nicosia (35.10°N, 33.30°E, 00Z) is also activated to fine tune the simulations. A series of sensitivity runs with various model configurations (different physical schemes, assimilation parameters and domain structures) is performed until we conclude to the optimum setup for the specific simulation.

2.2.2 Land use changes and activation of dust sources

An accurate representation of dust sources in the region is crucial for understanding this complex dust event, but this is hampered by seasonal and interannual variability of dust sources together with recent land cover changes in the region. The original land use database of the model is the USGS Data Base Version 2 which is obtained from 1-km AVHRR data (Advanced Very High Resolution Radiometer) spanning April 1992 through March 1993. Firstly, this annual-mean dataset cannot accurately describe the land use and dust sources at the end of the dry season in the Middle East. ~~Morover,~~ ~~However,~~Secondly, the complex interactions of drier climate (Notaro et al., 2015; Cook et al., 2016), transboundary water managements (Voss et al., 2013), and prolonged conflict (Jaafar and Woertz, 2016) have led to further changes of land use types that are no longer reflected at the model and this could have a large impact on dust production. The comparison of Landsat 8 natural color and NDVI imagery between August 2013 and 2015 (Figure 2) reveals large areas of uncultivated fields in regions of contested boarders and exposed river and lake-bed sediments especially around the Euphrates river, all of which are known to be very efficient dust sources (Prospero et al, 2002; Ginoux et al., 2012). The impact of the ongoing conflict on land use and vegetation can be further highlighted in Figure 3, showing the time series of MODIS NDVI in the region around Hawija, Kirkuk province, Iraq (region B of Fig.2). Agriculture in Hawija is based on a combination of rain-fed and irrigated fields, in accordance with a rainy and a dry season from November to May and from June to October respectively. The NDVI time series clearly captures this behavior, with a major annual NDVI pick during wet months and a smaller cycle during each summer, probably reflecting the growth of summer crops with the help of irrigation. This summer cycle is completely absent in 2015. Indeed, a recent survey of the Food and Agriculture Organization (FAO) of the United Nations, reveals that large parts of the irrigation system in Kirkuk and surrounding regions have been destroyed by military operations and a large number of pumps and generators required for irrigation have been stolen (Singh N. et al, 2016). This, together with the destruction of other agricultural equipment and

infrastructures, has severely disrupted the summer agriculture activities of 2015, exactly before the dust storm studied here, leaving the fields to act as very efficient dust sources.

In order to get most accurate representation of dust sources for the specific event we use 1km monthly Normalized Difference Vegetation Index (NDVI) from MODIS (Didan K., 2015) to characterize land use type in the region of interest. Specifically, we consider regions with NDVI values from 0 to 0.1 to correspond to bare soil and consequently efficient dust sources (DeFries et al., 1994). The updated land cover dataset is used for all results shown in this study. Results from simulations using the older database are only shown in Figure 11 for comparison.

3. Results

3.1 Meteorological conditions

The main driving force for the generation of this extreme dust episode is the combination ~~between~~ of two distinct meteorological features in the greater area: (i) establishment of a thermal low over the bare-soil areas of Syria and (ii) convective outflow boundaries at the mountains of Iraq and Syria. These processes are analyzed in the following sections using modeling results and remote sensing observations.

3.1.1 Development of a low pressure system over Syria on 6 September 2015

As seen at the outer model grid in Figure 1a, the passage of a trough is evident over Turkey on 6 September 2015, 00:00 UTC. The low pressure center at 500 mb is found at 5840 m over the east bank of Black Sea. During the same day, radiative warming of the bare soil surface results in very hot soil temperatures exceeding 50 °C in Syria and Iraq. Advection of warm air from the Red Sea is also evident at the lowest troposphere by the 1000-700 mb thickness in Figure 4a. This combination of cold air aloft with low level warming, leads in the formation of a thermal low pressure system over Syria that is evident by the 925 mb geopotential height in Figure 4b. Another parameter that plays important role for the process of dust source activation is the difference between surface temperature (T_{Surf}) and air temperature at 2m (T_{2m}). Findings from earlier field experiments (i.e. SAMUM) show that such a difference of 17°C-20°C facilitates the uplift of convective dust plumes (Ansmann et al., 2009). As seen in Figure 1b, the modeled T_{Surf}-T_{2m} difference at 10:00 UTC exceeds 17°C over extended bare soil areas in Syria. This temperature gradient further explains the

effectiveness of dust production at these areas. The pressure system and the associated cyclonic flow persist during the entire day of 6th September 2015 and result in the mobilization of dust in the area. ~~The low pressure system is evident by the 850 mb geopotential height contours in Figure 3a, reaching a minimum of 1490 m at 08:00 UTC, 6 September 2015.~~ Dust uptake is mostly evident at the outer parts of the cyclone where surface wind speed exceeds 7 m s^{-1} almost during the entire day and T_{Surf}-T_{2m} obtains maximum values. The elevated particles are quickly distributed inside the system and a distinct cylindrical dust cloud is soon formed. Recirculation of the elevated dust particles inside the closed cyclonic flow results in extreme AOT values exceeding 15 at specific areas as seen in Figure ~~3a~~4b. The formation of this dense dust plume is also evident in the MSG-SEVIRI satellite dust RGB image in Figure ~~3b~~4c. Pink and purple colors in this image indicate dust while brown and red colors indicate clouds. The convective outflows from the Zagros Mountains in Turkey that are evident by the black dashed line and wind vectors at 925 mb in Figure 3b enhance the mobilization of dust at the northern parts of the heat low. ~~As seen in Figure 4, convergence of low level flow along the Mediterranean coastline during the morning hours on September 6th, results in local convective activity at the area of Lebanon Mountains and in local disturbance of the mesoscale wind field. A SE flow is established, and this flow is responsible for the~~ ~~t~~. Transport of dust from Lebanon towards Cyprus ~~that~~ is evident at the satellite and modeling images on 7 September 2015, 00:00 UTC (Figure 5). This cut-off plume (plume_1) travels in the lower troposphere above the marine boundary layer and it was observed at 1.5 km above Limassol at 19:00 UTC on September 7th as reported by Mamouri et al.~~,~~(~~-~~2016). The faster propagating haboob plume (plume_2) ~~also~~ was detected at 2.0-3.5 km over Cyprus at 19:00 UTC. The extreme AOT values (>10) that are seen in Figure 5a over Syria result from the overlapping of cyclone-driven and haboob-driven dust over this area. In the model, ~~approaching~~ approach of the haboob front in Syria is accompanied also by cloud formation as seen by the 70% cloud-cover contours in Figure 5a; however these clouds are not evident in the satellite image (Figure 5b). The more elevated (cyclone-driven) dust in Figure 5b is shown in pink (plume_1 over the sea and plume_3 over Northern Syria and Southern Turkey have the same origin) and the near surface dust (haboob) is shown with a darker purple color (plume_2).

3.1.2. Convection and haboob generation on 6 and 7 September 2015

At 13:00 UTC on 6~~th of~~ September a northward low level flow is evident over N. Iraq and N. Syria (Figure 6a). This relatively unstable air mass is characterized by increased equivalent potential

temperature (theta_e) reaching up to 508 K. This flow is associated with a westerly shift of the Somalian Low Level Jet (SLLJ). The SLLJ is part of the West India Monsoon circulation and ~~as~~ is shown in Figure 6b. ~~I~~It is characterized by strong SW winds blowing from the Somali~~a~~ highlands towards West India. This low level flow steers towards the west along the coastal mountains of Yemen and Oman and results in SE winds transferring moisture from the Arabian Sea towards the inlands of the Arabian Peninsula. Low-level advection of warm towards the storm area also evident in Figure 6c by the 1000-700 mb modeled thickness at 15:00 UTC. Mechanical elevation of this relatively unstable air as it approaches Mt. Sinjar in N. Iraq (Figure 6a) triggers convection at this area. A number of atmospheric ~~crucial~~ parameters that determine~~s~~ the formation of ~~a~~ the cold pool are shown in Figures7a-d. ~~is the temperature difference between rain droplets and the ambient air.~~ As seen in Figure 7a, the iso-temperature line of -20°C ~~absolute difference~~ between rain droplets temperature and ambient air temperature in the model ~~reaches a maximum of 22 °C at this area~~ clearly defines the cold pool area. Sub-saturated air below the cloud base is also evident in Figure 7a since the relative humidity at the neighbor of the convective cloud is between 15-20 %. ~~This~~The combination of sub-saturated air and temperature gradient results in a faster evaporation rate of the rain droplets ~~as they fall through the unsaturated air~~ and in the formation of a cold pool at the area of Northern Iraq. ~~Wind~~ with speeds ~~inside the cold pool~~ ranginges from 10 up to 20 ms^{-1} (Figure 7b). The convective cloud top reaches 12 km and the updrafts exceed 18 m s^{-1} at 15:00 UTC (Figure 7c). The rainfall curtain (downdraft area in Figure 7c) extends up to 4-5 km and the severity of the storm leads in the formation of a haboob that is evident by the streamline structure and dust production below the non-precipitating parts of the cloud in Figure 7d. A Kelvin-Helmholtz billow at 2-3 km separates the density current head from the ambient flow similar to previous findings for convective haboobs (Solomos et al., 2012). Dust particles are distributed inside the system and dust concentrations exceed 2000 μg m^{-3} below the cloud. ~~This~~ As the cold pool moves towards the North ~~and~~ it triggers the generation of secondary convective cells at the mountainous areas along Iran-Iraq-Turkey borderline. At 20:00 UTC, a series of convective outflows converges in an organized SE propagating density current that is evident in the model over N. Iraq and N. Syria (Figure 8a). This system is characterized by wind speeds higher than 6 m s^{-1} and results in activation of dust sources and near surface modelled concentrations largely exceeding 10000 μg m^{-3} (Figure 8b). However, the corresponding SEVIRI image (Figure 8c) indicates that by this time the haboob has already penetrated about 200 km inside Syria which is not reproduced by the model. The latency between satellite and modeled haboob fronts is possibly

attributed to a slower propagating modeled haboob or to a triggering delay of convection in the model due to the imperfect representation of boundary layer properties and atmospheric stability. ~~This latency between satellite and modeled haboob fronts is an indication that the convective downdrafts were in fact even stronger.~~

3.2 Dust cloud properties and comparison with observations

3.2.1. Vertical dust structure

The dust layer structure as it propagates towards the Mediterranean is captured by two CALIPSO overpasses at 23:33 UTC, 6 September 2015 (Figure 9) and at 10:35 UTC, 7 September 2015 (Figure 10). Collocated model cross sections of dust and MSG-SEVIRI dust images are also presented in Figures 9~~8~~ and 10~~9~~. All heights in satellite and model profiles refer to heights above surface. At the first overpass (Figure 9), the southern part of the dust layer (31°N-34°N) is detected up to 2-3 km and originates from the cyclonic flow over Syria. The modeled dustload is also shown in Figure 9b for comparison. Dust concentrations are estimated from CALIPSO lidar signal ~~-~~backscatter and as seen in Figure 9c~~b~~ they reach up to 5000 μg m^{-3} close to the surface between 31°N-34°N and higher than 6000 μg m^{-3} in the first 500 m. Similar structure and dust concentrations are also found by the model (Figure 9d~~c~~). The northern part of the overpass (35°N-38°N) detects also elevated dust due to cyclonic activity between 2.5-4.5 km and concentrations up to 1000-2000 μg m^{-3} are evident at this area from CALIPSO. The model overpredicts dust at this area with simulated concentrations reaching up to 5000 μg m^{-3}. These elevated layers are shown with pink colors in Figure 9a. Low level dust (purple colors in SEVIRI images) is also evident in this area due to the propagating haboob and CALIPSO detects this two-layer structure with a clear separation at 2 km. The model also reproduces the uplift of dust at 35°N where the two systems (cyclone and haboob) merge. The modeled concentration inside the haboob reaches extraordinary values exceeding 10000 μg m^{-3}. Due to the severity of the event, the CALIPSO lidar signal is totally attenuated ~~bellow~~ below ~1 km (dark blue color), in the area between 35°N-37°N. For that reason the information from the satellite is limited ~~there~~ at this area in the ~~highest~~ top 500m of the propagated haboob (1-1.5 km), implying also the existence of much higher values close to the surface.

The second overpass at 7 September 10:35 UTC is actually behind or at the tail of the propagating dust storm (Figure 10a). The modeled dustload is also shown in Figure 10b for comparison. The thin dust layer that is detected by CALIPSO between 30°N-32°N reaches up to 2 km and maximum dust

concentrations of up to 2000-3000 μg m^{-3} are calculated mostly close to the surface (Figure ~~10b~~10c). Extreme dust concentrations are also found in both satellite and model plots between 34°N-36°N at the tail of the propagating system. Dust values at this area are so high that CALIPSO observation again suffers ~~again~~ from total attenuation of the lidar signal after penetrating the first 1000 m and extraordinary concentrations of up to 20000 μg m^{-3} are found in the lower model levels (up to 1.5 km). Similar values are observed from CALIPSO ~~in~~ at the edge of the haboob (33.5°N-34°N) where the signal is strong enough to provide valuable information. The elevated layers (2-4 km) between 36°N-38°N at both CALIPSO and model profiles are dust residuals over the mountains of Turkey. An elevated dust layer of up to 600 μg m^{-3} is also found south of 35°N in the model at heights between 3-4 km. Due to the aforementioned latency between the true and modeled propagation speeds, the model cross-section is closer to the core of the system hence this layer consists of modeled cyclone uplifted dust that in fact is already west of the CALIPSO ground track.

3.2.2. Dust load over Cyprus

The observed structure and amounts of dust arriving in Cyprus is described in detail by Mamouri et al. (2016). The arrival of the dust plumes at Limassol in Cyprus is evident in Figure 11. A double layer structure is detected by the lidar ~~at~~ on 7 September 19:00 UTC. The relatively shallow dust layer that is found between 0.8-1.7 km with a maximum peak at 2000 μg m^{-3}, comes from the detached dust air mass traveling off the coast of ~~Libanon~~ Lebanon as described in Section 3.1.1. The model reproduces correctly the height of this layer but the maximum concentration is underestimated by almost 50 %. The upper layer that is detected between 1.8-3.6 km originates from the north part of the fast propagating haboob that catches up with the "Lebanon" dust over Cyprus. The location and dust concentrations of this layer are adequately reproduced by the model. The total modeled dust load is similar to the observed (lidar) dust load but the vertical distribution of dust in two distinct layers is not so clearly reproduced. Model results using the old vegetation database are also shown in Figure 11. As seen by the dashed line in this plot, this simulation failed to reproduce the strength of the event and the maximum concentration is 400 μg m^{-3} at about 0.7 km height. On ~~the~~ 8~~th~~ ~~of~~ September the lidar system could not operate due to the extraordinary dust load. The mean MODIS derived AOT on this day varied between 1.5-5 over five sites in Cyprus (Pafos, Limassol, Larnaca, Nicosia, Rizokarpaso), (Mamouri et al., 2016). Given the fact that the maximum retrievable MODIS AOT is 5, these values are most probably an underestimation of the true AOT. The distribution of modeled AOT during 00:00

UTC-15:00 UTC on ~~the~~ 8~~th of~~ September is shown in Figure12; the dust plume approaches Cyprus from the South and the orographic effect of Mt. Troodos results in an inhomogeneous distribution of dustload over the island, which explains the AOT variability between the sites. The modeled AOT values over the Middle East inland exceed 10 as shown also by the sharp gradient towards the eastern part of Figure 12 plots. However the extreme dust storm affecting Cyprus during ~~the~~ 8~~th of~~ September is the result of a plume that approaches the island from the south. This dust layer is evident between 1.5-3.5 km in the vertical cross-sections of model dust concentration at 00:00 UTC and 03:00 UTC in Figure 13. Differential heating between the land and water bodies and between flat terrain and mountain slopes results in the development of local wind flows (downslope / upslope winds). Downward mixing of dust as this air mass approaches the topographic barrier of Troodos mountain increases the near-surface concentrations at the southern sites especially during local morning and noon hours (06:00 UTC, 09:00 UTC). In the afternoon hours (12:00 UTC, 15:00 UTC), the development of upward motions over Mt. Troodos separates the dust flow over Cyprus into two distinct cells (a south and a north one) and at this time increased concentrations are found over the northern sites of the island. The maximum simulated concentrations are up to 4000 μg m^{-3} aloft and about 1000 μg m^{-3} close to the surface.

Taking into account the complexity of the situation, the spatiotemporal evolution of the episode seems to be correctly explained by the model but the extreme values of 8000-10000 mg m^{-3} that are reported by Mamouri et al. (2016) are not reproduced. This discrepancy can be attributed to a variety of reasons related to both dust and atmospheric properties that are not properly resolved even at this fine model scale (e.g. more intense downward mixing, ~~or~~ increased emissions from the sources, limitations due to emission size bins, inaccurate deposition rates etc.). The modeled versus observed maximum AOT values for the five sites are also shown in Table ~~1~~2. The model reproduces the higher AOTs at the most southern sites (Limassol and Pafos) compared to the central and north sites. Following the previous discussion about the already underestimated MODIS AOT it seems that the model reproduces the distribution of dust over Cyprus however with an overall underestimation of more than 2. A possible explanation could be also that the dry river beds of Tigris and Euphrates as well as several dust sources over Syria and North Iraq provide even more erodible sediments than those assumed by the model hence the discrepancies in dust concentrations.

~~Table 1. Maximum MODIS and RAMS AOT over Cyprus, 8 September 2015~~

	~~Pafos~~	~~Limassol~~	~~Larnaca~~	~~Nicosia~~	~~Rizokarpaso~~
~~$MODIS_{AOT}$~~	~~3.5~~	~~5.0~~	~~5.0~~	~~2.0~~	~~5.0~~
~~$RAMS_{AOT}$~~	~~3.5~~	~~4.0~~	~~3.0~~	~~3.0~~	~~3.0~~

4. Discussion and Conclusions

A combination of meteorological and landuse conditions resulted in the formation of an unprecedented dust episode over Middle East and the Eastern Mediterranean during 6-11 September 2015. This event is unique due to the coincidence of various atmospheric phenomena related with the generation of turbulence and dust production. Interpretation and analysis of remote sensing data (EARLINET, CALIPSO, MSG-SEVIRI) and modeling simulations (RAMS-ICLAMS) reveals the main reasons that led in the uplift and persistence of the dust layers.

The major processes affecting the generation of the dust storm are found to be:

1. The formation of strong thermal low and convective outflows over Syria that lifted dust up to 4 km.
2. The intrusion of ~~a moist and unstable air mass~~ from the moist and unstable air masses Arabian Sea and the Red Sea that triggered convective activity over Iraq-Iran-Syria-Turkey borderline.
3. The generated outflow boundaries that led in dust deflation and formed a westward propagating haboob merging with the previously elevated dust over Syria.
4. The efficiency of Middle East dust sources is increased as an aftermath of war and the related changes in land use.

As reported by Mamouri et al. (2016), almost all operational dust models failed to forecast this event. RAMS-ICLAMS in this study is not used in forecasting mode but rather as a tool for the a-posteriori analysis and explanation of the event. This means that the configuration of several model parameters such as the nested grid structure, convective parameterization schemes, dust source strength etc. is guided by the available observations. In this context, most observed processes are successfully described by the model and the various physical mechanisms that took place during the event are

explained. However, certain inaccuracies in the quantification of atmospheric variables and spatiotemporal deviations in the description of convection and other physical processes can still significantly decrease the model skill especially regarding the quantification of dust mass profiles.

The analysis presented here raises considerations regarding the forecast skill~~s~~ of the atmospheric dust models, since even though such extreme episodes are ~~very~~ seldom, they still represent the most threatening dust hazards. The long range transport and the general circulation of dust in the atmosphere are ~~nowadays~~ now often adequately forecasted by most global models but convectively driven episodes cannot be resolved at synoptic and mesoscale resolutions. Moreover, a recent study by Pope et al.~~,~~ (2016) at the area of Sahel/southern Sahara suggests that unresolved haboobs during the summer monsoon may be responsible for up to 30% of the total atmospheric dust and such considerations raise questions on the current status of early warning systems for dust episodes. It is probably obvious that such a system cannot rely exclusively on modeling simulations. As shown at the present study, the complexity of these events makes ~~their~~ forecasting them very challenging and even at convection permitting resolutions.~~,~~ As shown at the present study, the complexity of these events makes forecasting them very challenging and it is possible that a certain model configuration could successfully reproduce a specific event but not all similar events. ~~it is possible that a certain model configuration could successfully reproduce a specific event but not all similar events.~~ The key for forecasting these events in atmospheric models is the use of cloud resolving grid space. However, such high resolution grid-space can only be applied over limited areas due to restrictions in computational power. ~~Moreover, such high resolution grid-space can only be applied over limited areas due to restrictions in computational power.~~ Forthcoming studies using an extended cloud-resolving grid over the entire Middle-East (e.g. Gasch et al., 2017) could provide more detail on the individual atmospheric processes during this episode.

Remote sensing observations can play an important role for the provision of more accurate dust forecasts. Engagement of geostationary satellite observations (MSG, Sentinel-4) and CALIPSO profiles in forecasting activities could improve the forecasting skill either by the direct assimilation of satellite data in dust models or by issuing human-assisted early warnings. Expansion of a lidar network close to dust source areas (e.g. Sahara, Middle East) will also complement model activities through the provision of ground truth observations for the vertical profile of dust plumes. Additionally, the activation of ~~synchronous~~ correlated observations from the EARLINET network following a dust forecast notice will allow a closer investigation of the physical processes that drive these events.

.

Acknowledgements

The authors acknowledge support through the following projects and research programs: BEYOND under grant agreement no. 316210 of the European Union Seventh Framework Programme FP7-REGPOT-2012-2013-1. ACTRIS-2 under grant agreement no. 654109 of the European Union's Horizon 2020 research and innovation programme. ECARS under grant agreement No 602014 from the European Union's Horizon 2020 Research and Innovation programme. MarcoPolo under grant agreement no. 606953 of the European Union Seventh Framework Programme FP7/2007-2013. The authors acknowledge EARLINET for providing aerosol lidar profiles available under the World Data Center for Climate (WDCC) (The EARLINET publishing group 2000-2010, 2014a. CALIPSO data were obtained from the ICARE Data Center (http://www.icare.univ-lille1.fr/) and from the NASA Langley Research Center Atmospheric Science Data Center. CALIPSO data were provided by NASA. We thank the ICARE Data and Services Center for providing access to the data used in this study and their computational center.

References

Ansmann A., Tesche, M., Knipperts, P., Bierwirth, E., Althausen, D., Muller, D. and Schulz. O.: Vertical profiling of convective dust plumes in southern Morocco during SAMUM. Tellus 61B, doi:10.1111/j.1600-0889.2008.00384.x., 2009

Ansmann, A., Petzold, A., Kandler, K., Tegen, I., Wendisch, M., Müller, D., Weinzierl, B., Müller, T., and Heintzenberg, J.: Saharan Mineral Dust Experiments SAMUM-1 and SAMUM-2: what have we learned?, Tellus, 63B, 403–429, 2011

Ansmann, A., Seifert, P., Tesche, M., and Wandinger, U.: Profiling of fine and coarse particle mass: case studies of Saharan dust and Eyjafjallajökull/Grimsvötn volcanic plumes, Atmos. Chem. Phys., 12, 9399–9415, doi:10.5194/acp-12-9399-2012, 2012.

Banks, J. R. and Brindley, H. E.: Evaluation of MSG-SEVIRI mineral dust retrieval products over North Africa and the Middle East, Remote Sensing of Environment, 128, 58–73, doi:10.1016/j.rse.2012.07.017, 2013.

Barahona, D., West, R. E. L., Stier, P., Romakkaniemi, S., Kokkola, H., and Nenes, A.: Comprehensively accounting for the effect of giant CCN in cloud activation parameterizations, Atmos. Chem. Phys., 10, 2467–2473, doi:10.5194/acp-10-2467-2010, 2010.

Benedetti A., J.-J., Morcrette, O. Boucher, A. Dethof, R. J. Engelen, M. Fisher, H. Flentje, N. Huneeus, L. Jones, J. W. Kaiser, S. Kinne, A. Mangold, M. Razinger, A. J. Simmons, and M. Suttie: Aerosol analysis and forecast in the European Centre for Medium-Range Weather Forecasts Integrated Forecast System: 2. Data assimilation, J. Geophys. Res., 114, D13205, doi:10.1029/2008JD011115., 2009

Bou Karam, D., Flamant, C., Knippertz, P., Reitebuch, O., Pelon, J., Chong, M., and Dabas, A: Dust emissions over the Sahel associated with the West African Monsoon inter-tropical discontinuity region: a representative case study, Q. J. Roy. Meteor. Soc., 134, 621–634, 2008.

Brindley, H., Knippertz, P., Ryder, C. and Ashpole, I.: A critical evaluation of the ability of the Spinning Enhanced Visible and Infrared Imager (SEVIRI) thermal infrared red-green-blue rendering to identify dust events: Theoretical analysis, J. Geophys. Res., 117(D7), D07201, doi:10.1029/2011JD017326, 2012.

Cook, B. I., Anchukaitis, K. J., Touchan, R., Meko, D. M. and Cook, E. R.: Spatiotemporal drought variability in the Mediterranean over the last 900 years, J. Geophys. Res. Atmos., 121(5), 2015JD023929, doi:10.1002/2015JD023929, 2016.

Cotton W. R., Pielke Sr., R. A., Walko, R. L., Liston, G. E., Tremback, C. J., Jiang, H., McAnelly, R. L., Harrington, J. Y., Nicholls, M. E., Carrio, G. G., and McFadden, J. P.: RAMS 2001: Current status and future directions, Meteor. Atmos. Phys., 82, 5–29, 2003

DeFries, R. S. and Townshend, J. R. G.: NDVI-derived land cover classifications at a global scale, International Journal of Remote Sensing, 15(17), 3567–3586, doi:10.1080/01431169408954345, 1994.

Didan, K: MOD13A3 MODIS/Terra vegetation Indices Monthly L3 Global 1km SIN Grid V006, , doi:10.5067/MODIS/MOD13A3.006, 2015.

Emmel C, Knippertz P, Schulz O (2010) Climatology of convective density currents in the southern foothills of the Atlas mountains. J Geophys Res 115, D11115. doi:10.1029/2009JD011819

Fountoukis, C., Nenes, A., Meskhidze, N., Bahreini,, R., Conant, W. C., Jonsson, H., Murphy, S., Sorooshian, A., Varutbangkul, V., Brechtel, F., Flagan, R. C., and Seinfeld, J. H.: Aerosol – cloud drop concentration closure for clouds sampled during the International Consortium for Atmospheric Research on Transport and Transformation 2004 campaign, J. Geophys. Res., 112, D10S30, doi:10.1029/2006JD007272, 2007.

Gasch, P., Rieger, D., Walter, C., Khain, P., Levi, Y., and Vogel, B.: An analysis of the September 2015 severe dust event in the Eastern Mediterranean, Atmos. Chem. Phys. Discuss., doi:10.5194/acp-2017-11, in review, 2017.

Ginoux, P., Prospero, J. M., Gill, T. E., Hsu, N. C. and Zhao, M.: Global-scale attribution of anthropogenic and natural dust sources and their emission rates based on MODIS Deep Blue aerosol products, Rev. Geophys., 50(3), RG3005, doi:10.1029/2012RG000388, 2012.

Gong, S. L., Barrie, L. A., and Lazare, M.: Canadian Aerosol Module (CAM): a size-segregated simulation of atmospheric aerosol processes for climate and air quality models. 2. Global seasalt aerosol and its budgets,

J. Geophys. Res., 107(D24), 4779, doi:10.1029/2001JD002004, 2002.

Gong, S. L.: A parameterization of sea-salt aerosol source function for sub- and super-micron particles, Global Biogeochem. Cy., 17, 1097, doi:10.1029/2003GB002079, 2003.

Iacono, M. J., Mlawer, E. J., Clough, S. A., and Morcrette, J. J.: Impact of an improved longwave radiation model, RRTM, on the energy budget and thermodynamic properties of the NCAR Community Climate Model, CCM3, J. Geophys. Res., 105, 14873– 14890, 2000

Jaafar, H. H. and Woertz, E.: Agriculture as a funding source of ISIS: A GIS and remote sensing analysis, Food Policy, 64, 14–25, doi:10.1016/j.foodpol.2016.09.002, 2016.

Kain, J. S. and Fritsch, J. M.: Convective parameterization for mesoscale models: The Kain-Fritsch scheme. The representation of cumulus convection in numerical models, Meteor. Monogr., No. 24, Amer. Meteor. Soc., 165–170, 1993.

Knippertz P, Trentmann J. Seifert A., High resolution simulations of convective cold pools over the northwestern Sahara. J. Geophys. Res. 2009; 114:D21109. doi: 10.1029/2007JD008774., 2009

Leeuw, G., Neele, F. P., Hill, M., Smith, M. H., and Vignali, E.: Production of sea spray aerosol in the surf zone, J. Geophys. Res.- Atmos., 105, 29397–29409, 2000.

Lensky I.M. and D. Rosenfeld, 2008: Clouds-Aerosols-Precipitation Satellite Analysis Tool (CAPSAT). Atmos. Chem. Phys., 8, 6739–6753.

Mamouri, R. E., Ansmann, A., Nisantzi, A., Kokkalis, P., Schwarz, A., and Hadjimitsis, D.: Low Arabian dust extinctionto-backscatter ratio, Geophys. Res. Lett., 40, 4762–4766,doi:10.1002/grl.50898, 2013.

Mamouri R.E., Ansmann, A., Nisantzi, A., Solomos, S., Kallos, G., and Hadjimitsis, D.G.: Extreme dust storm over the eastern Mediterranean in September 2015: satellite, lidar, and surface observations in the Cyprus region Atmos. Chem. Phys., 16, 1–14, 2016 www.atmos-chem-phys.net/16/1/2016/doi:10.5194/acp-16-1-2016.

Mamouri, R.E. and Ansmann, A.: Fine and coarse dust separation with polarization lidar: Extended Methodology for multiple wavelengths, to be submitted to ACP, 2017.

Marsham, J. H., N. S. Dixon, L. Garcia-Carreras, G. M. S. Lister, D. J. Parker, P. Knippertz, and C. E. Birch : The role of moist convection in the West African monsoon system: Insights from continental-scale convection-permitting simulations, Geophys. Res. Lett., 40, 1843–1849, doi:10.1002/grl.50347., 2013

Marticorena, B. and Bergametti, G.: Modeling the atmospheric dust cycle: 1. Design of a soil derived dust emission scheme, J. Geophys. Res., 100, 16415–16430, 1995.

Meyers, M. P., Walko, R. L., Harrington, J. Y., and Cotton, W. R: New RAMS cloud microphysics parameterization. Part II: The two-moment scheme, Atmos. Res., 45, 3–39, 1997

Mlawer, E. J., Taubman, S. J., Brown, P. D., Iacono, M. J., and Clough, S. A.: Radiative transfer for inhomogeneous atmospheres: RRTM, a validated correlated-k model for the longwave, J. Geophys. Res.,

102(D14), 16663–16682, 1997.

Mona L., Z. Liu, D. Müller, A. Omar, A. Papayannis, G. Pappalardo, N. Sugimoto and M. Vaughan, "Lidar Measurements for Desert Dust Characterization: An Overview," Advances in Meteorology, vol. 2012, Article ID 356265, 36 pages, 2012. doi:10.1155/2012/356265

Monahan, E. C., Spiel, D. E., and Davidson, K. L.: A model of marine aerosol generation via whitecaps and wave disruption, in: Oceanic Whitecaps, edited by: Monahan, E. C. and Mac Niocaill, G., D. Reidel, 167–174, 1986.

Notaro, M., Yu, Y. and Kalashnikova, O. V.: Regime shift in Arabian dust activity, triggered by persistent Fertile Crescent drought, J. Geophys. Res. Atmos., 120(19), 2015JD023855, doi:10.1002/2015JD023855, 2015.

Pielke, R. A., Cotton, W. R., Walko, R. L., Tremback, C. J., Lyons, W. A., Grasso, L. D., Nicholls, M. E., Moran, M. D., Wesley, D. A., Lee, T. J., and Copeland, J. H.: A comprehensive meteorological modeling system – RAMS, Meteorol. Atmos. Phys., 49, 69–91, 1992.

Pope, R. J., J. H. Marsham, P. Knippertz, M. E. Brooks, and A. J. Roberts: Identifying errors in dust models from data assimilation, Geophys. Res. Lett., 43, 9270–9279, doi:10.1002/2016GL070621., 2016

Prospero, J. M., Ginoux, P., Torres, O., Nicholson, S. E. and Gill, T. E.: Environmental Characterization of Global Sources of Atmospheric Soil Dust Identified with the Nimbus 7 Total Ozone Mapping Spectrometer (toms) Absorbing Aerosol Product, Rev. Geophys., 40(1), 1002, doi:10.1029/2000RG000095, 2002.

Reinfried, F., I. Tegen, B. Heinold, O. Hellmuth, K. Schepanski, U. Cubasch, H. Huebener, and P. Knippertz : Simulations of convectively-driven density currents in the Atlas region using a regional model: Impacts on dust emission and sensitivity to horizontal resolution and convection schemes, J. Geophys. Res., 114, D08127, doi:10.1029/2008JD010844., 2009

Roberts, A. J., P. Knippertz : The formation of a large summertime Saharan dust plume: Convective and synoptic-scale analysis, J. Geophys. Res. Atmos., 119, 1766–1785, doi:10.1002/2013JD020667., 2014

Ryder, C. L., McQuaid, J. B., Flamant, C., Rosenberg, P. D., Washington, R., Brindley, H. E., Highwood, E. J., Marsham, J. H., Parker, D. J., Todd, M. C., Banks, J. R., Brooke, J. K., Engelstaedter, S., Estelles, V., Formenti, P., Garcia-Carreras, L., Kocha, C., Marenco, F., Sodemann, H., Allen, C. J. T., Bourdon, A., Bart, M., Cavazos-Guerra, C., Chevaillier, S., Crosier, J., Darbyshire, E., Dean, A. R., Dorsey, J. R., Kent, J., O'Sullivan, D., Schepanski, K., Szpek, K., Trembath, J., and Woolley, A.: Advances in understanding mineral dust and boundary layer processes over the Sahara from Fennec aircraft observations, Atmos. Chem. Phys., 15, 8479–8520, doi:10.5194/acp-15-8479- 2015, 2015

Schepanski, K., Tegen, I., Todd, M. C., Heinold, B., Bonisch, G., Laurent, B., and Macke, A.: Meteorological processes forcing Saharan dust emission inferred from MSG-SEVIRI observations of subdaily dust source activation and numerical models, J. Geophys. Res., 114, D10201, doi:10.1029/2008JD010325, 2009.

Seinfeld, J. H. and Pandis, S. N.: Atmospheric Chemistry and Physics: From Air Pollution to Climate Change, J. Wiley, New York, 1998

Singh N., van Zoonen D., and Khogir M.: Iraq agriculture and livelihoods needs assessment in the newly liberated areas of Kirkuk, Ninewa and Salahadin, Food and Agricutlure Organization of the United Nations, 2016.

Solomos, S., Kallos, G., Kushta, J., Astitha, M., Tremback, C., Nenes, A., and Levin, Z.: An integrated modeling study on the effects of mineral dust and sea salt particles on clouds and precipitation, Atmos. Chem. Phys., 11, 873–892, doi:10.5194/acp- 11-873-2011, 2011

Solomos, S., Kallos, G., Mavromatidis, E., and Kushta, J.: Density currents as a desert dust mobilization mechanism, Atmos. Chem. Phys., 12, 11199-11211, doi:10.5194/acp-12-11199-2012, 2012.

Spyrou, C., Mitsakou, C., Kallos, G., Louka, P., and Vlastou, G.: An improved limited-area model for describing the dust cycle in the atmosphere, J. Geophys. Res., 115, D17211, doi:10.1029/2009JD013682, 2010.

Takemi, T.: Explicit simulations of convective-scale transport of mineral dust in severe convective weather, J. Meteorol. Soc. Jpn., 83A, 187–203, 2005.

Takemi, T.: Structure and evolution of a severe squall line over the arid region in Northwest China. Mon. Wea. Rev., 127, 1301–1309., 1999.

The EARLINET publishing group 2000–2010: Adam, M., Alados-Arboledas, L., Althausen, D., Amiridis, V., Amodeo, A., Ansmann, A., Apituley, A., Arshinov, Y., Balis, D., Belegante, L., Bobrovnikov, S., Boselli, A., Bravo-Aranda, J. A., Bösenberg, J., Carstea, E., Chaikovsky, A., Comerón, A., D'Amico, G., Daou, D., Dreischuh, T., Engelmann, R., Finger, F., Freudenthaler, V., Garcia-Vizcaino, D., García, A. J. F., Geiß, A., Giannakaki, E., Giehl, H., Giunta, A., de Graaf, M., Grana-dos-Muñoz, M. J., Grein, M., Grigorov, I., Groß, S., ruening, C., Guerrero-Rascado, J. L., Haeffelin, M., Hayek, T., Iarlori, M., Kanitz, T., Kokkalis, P., Linné, H., Madonna, F., Mamouri , R.-E., Matthias, V., Mattis, I., Menéndez, F. M., Mitev, V., Mona, L., Morille, Y., Muñoz, C., Müller, A., Müller, D., Navas-Guzmán, F., Nemuc, A., Nicolae, D., Pandolfi, M., Papayannis, A., Pappalardo, G., Pelon, J., Perrone, M. R., Pietruczuk, A., Pisani, G., Potma, C., Preißler, J., Pujadas, M., Putaud, J., Radu, C., Ravetta, F., Reigert, A., Rizi, V., Rocadenbosch, F., Rodríguez, A., Sauvage, L., Schmidt, J., Schnell, F., Schwarz, A., Seifert, P., Serikov, I., Sicard, M., Silva, A. M., Simeonov, V., Siomos, N., Sirch, T., Spinelli, N., Stoyanov, D., Talianu, C., Tesche, M., De Tomasi, F., Trickl, T., Vaughan, G., Volten, H., Wagner, F., Wandinger, U., Wang, X., Wiegner, M., and Wilson, K. M.: EARLINET all observations (2000–2010), World Data Center for Climate (WDCC), doi:10.1594/WDCC/EN_all_measurements_2000-2010, 2014a.

Voss, K. A., Famiglietti, J. S., Lo, M., de Linage, C., Rodell, M. and Swenson, S. C.: Groundwater depletion in the Middle East from GRACE with implications for transboundary water management in the Tigris-Euphrates-Western Iran region, Water Resour. Res., 49(2), 904–914, doi:10.1002/wrcr.20078, 2013.

Vukovic, A., Vujadinovic, M., Pejanovic, G., Andric, J., Kumjian, M. R., Djurdjevic, V., Dacic, M., Prasad, A. K.,

El-Askary, H. M., Paris, B. C., Petkovic, S., Nickovic, S., and Sprigg, W. A.: Numerical simulation of "an American haboob", Atmos. Chem. Phys., 14, 3211-3230, doi:10.5194/acp-14-3211-2014, 2014.

Zhang, K. M., Knipping, E. M., Wexler, A. S., Bhave, P. V., and Tonnesen, G. S.: Size distribution of sea-salt emissions as a function of relative humidity, Atmos. Environ., 39, 3373–3379, 2005.

Table 1. Range and gamma correction for the Red, Green, and Blue channels for construct the Dust RGB product.

Color	SEVIRI Channels	Min (K)	Max (K)	Γ
Red	IR12.0 – IR10.8	-4	2	1
Green	IR10.8 – IR8.7	0	15	2.5
Blue	IR10.8	261	289	1

Table 2. Maximum MODIS and RAMS AOT over Cyprus (8 September 2015)

	Pafos	Limassol	Larnaca	Nicosia	Rizokarpaso
$MODIS_{AOT}$	3.5	5.0	5.0	2.0	5.0
$RAMS_{AOT}$	3.5	4.0	3.0	3.0	3.0

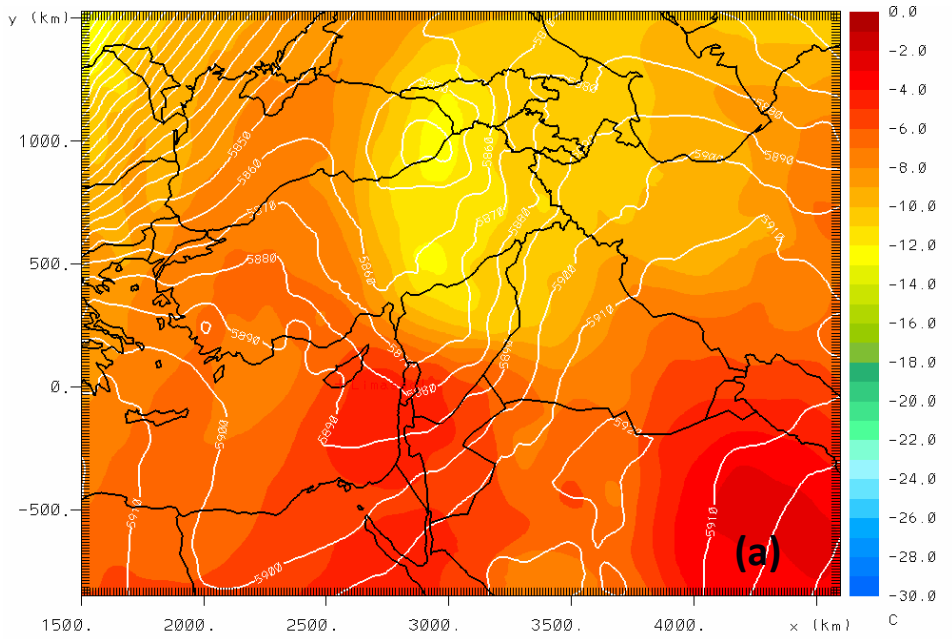
y (km)
1000.
500.
0.
-500.
1500.
2000.
2500.
3000.
3500.
4000.
x (km)
0.0
-2.0
-4.0
-6.0
-8.0
-10.0
-12.0
-14.0
-16.0
-18.0
-20.0
-22.0
-24.0
-26.0
-28.0
-30.0
C
(a)

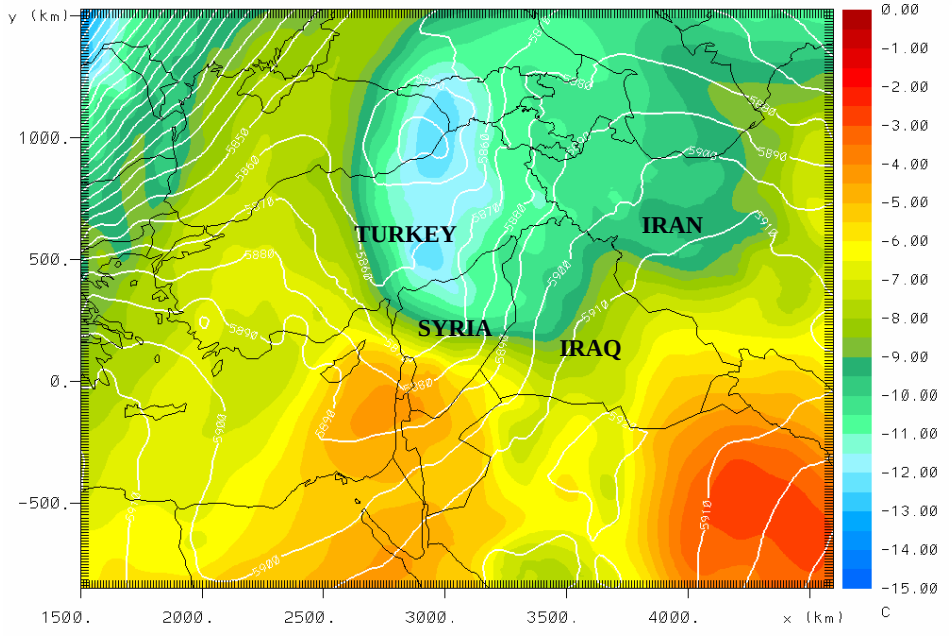
y (km)
1000.
500.
0.
-500.
1500.
2000.
2500.
3000.
3500.
4000.
x (km)
0.00
-1.00
-2.00
-3.00
-4.00
-5.00
-6.00
-7.00
-8.00
-9.00
-10.00
-11.00
-12.00
-13.00
-14.00
-15.00
C
TURKEY
IRAN
SYRIA
IRAQ

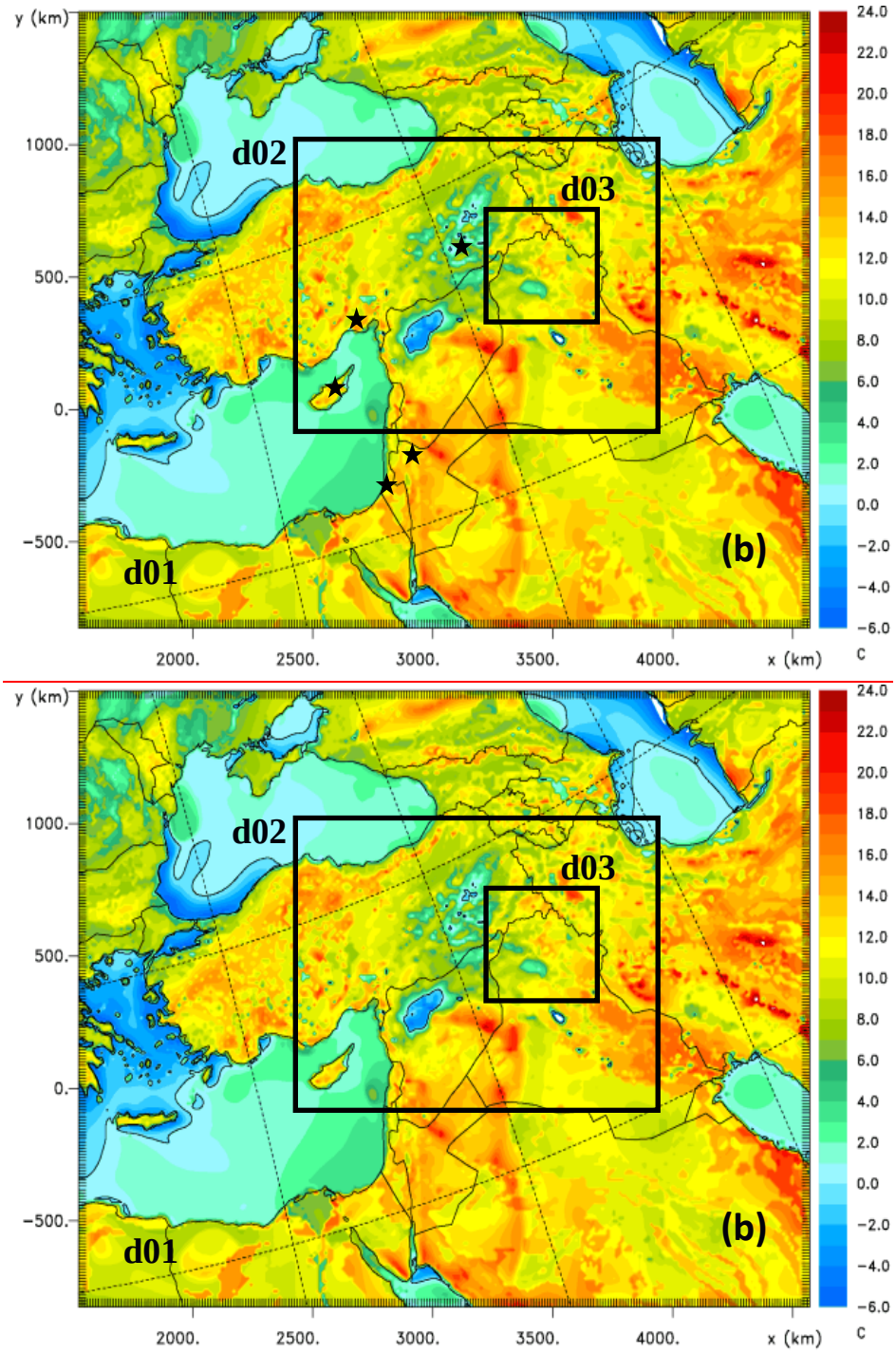

Figure 1. a) Model geopotential height contours (every 10 m) and temperature (color scale in °C) at 500mb, 6 September 2015, 00:00 UTC; b) Difference (°C) between model soil temperature and model temperature at 2m, 10:00 UTC, 6 September 2015. Black rectangulars indicate the location of the nested model domains (d01:12×12 km, d02:4×4 km, d03:2×2 km) and black stars the location of radiosondes.

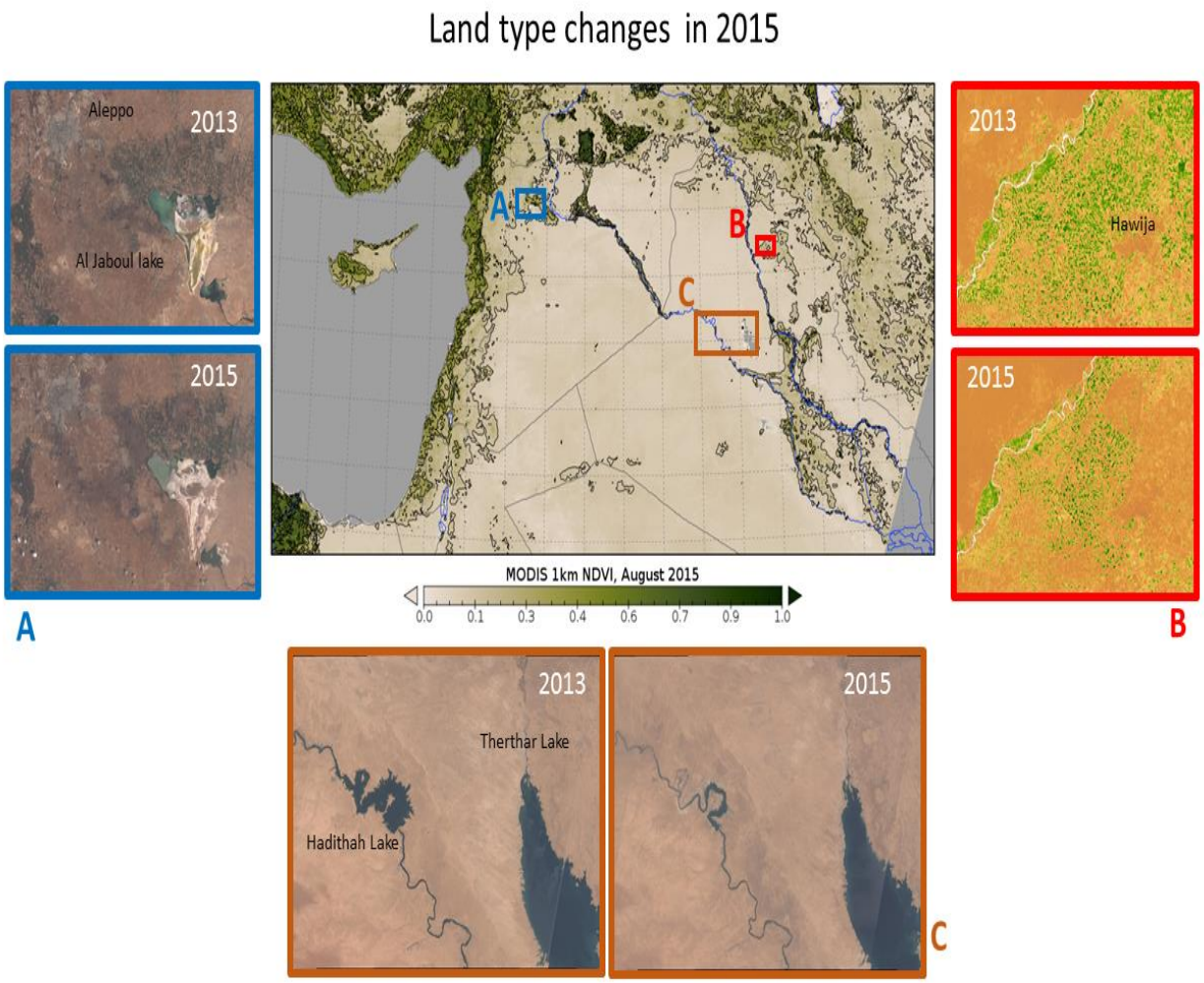

Figure 2. (central panel) MODIS NDVI observations for August 2015 were used to identify regions of bare soil that can be sources of dust aerosols. The contour lines correspond to the major ticks of the color scale. Large regions of wester Syria and Iraq have NDVI values from 0 to 0.1. The three subpanels show examples of land type change between summer 2013 and summer 2015. (Subpanel A) Landsat 8 natural color images of Aleppo region, Syria shows changes of cultivation patterns and drying of nearby Al Jaboul lake (e.g. the bright areas of the Al Jaboul Lake - dry parts of the lake - increased from 2013 to 2015); (Subpanel B) Landsat 8 NDVI index images in the region of Hawija, Kirkuk Province, Iraq reveal that large areas remained uncultivated in 2015 (e.g. the 2013 map shows many more green spots - agriculturally used areas - than the 2015 map); (Subpanel C) Landsat 8 natural color images showing diminishing area of Haditah Lake on the Euphrates river and the drying up of the Therthar canal and lake.

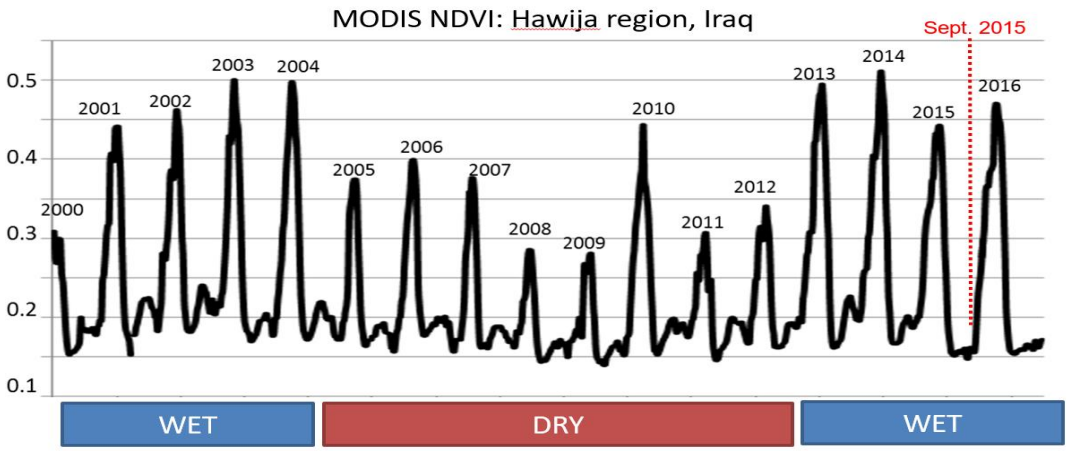

Figure 3. Time series of 16-day NDVI for the agricultural region around Hawija, Kirkuk province, Iraq. The vertical dashed lined marks the time of the studied dust storm. Note the absence of NDVI variation in the summer of 2015, prior to the dust storm.

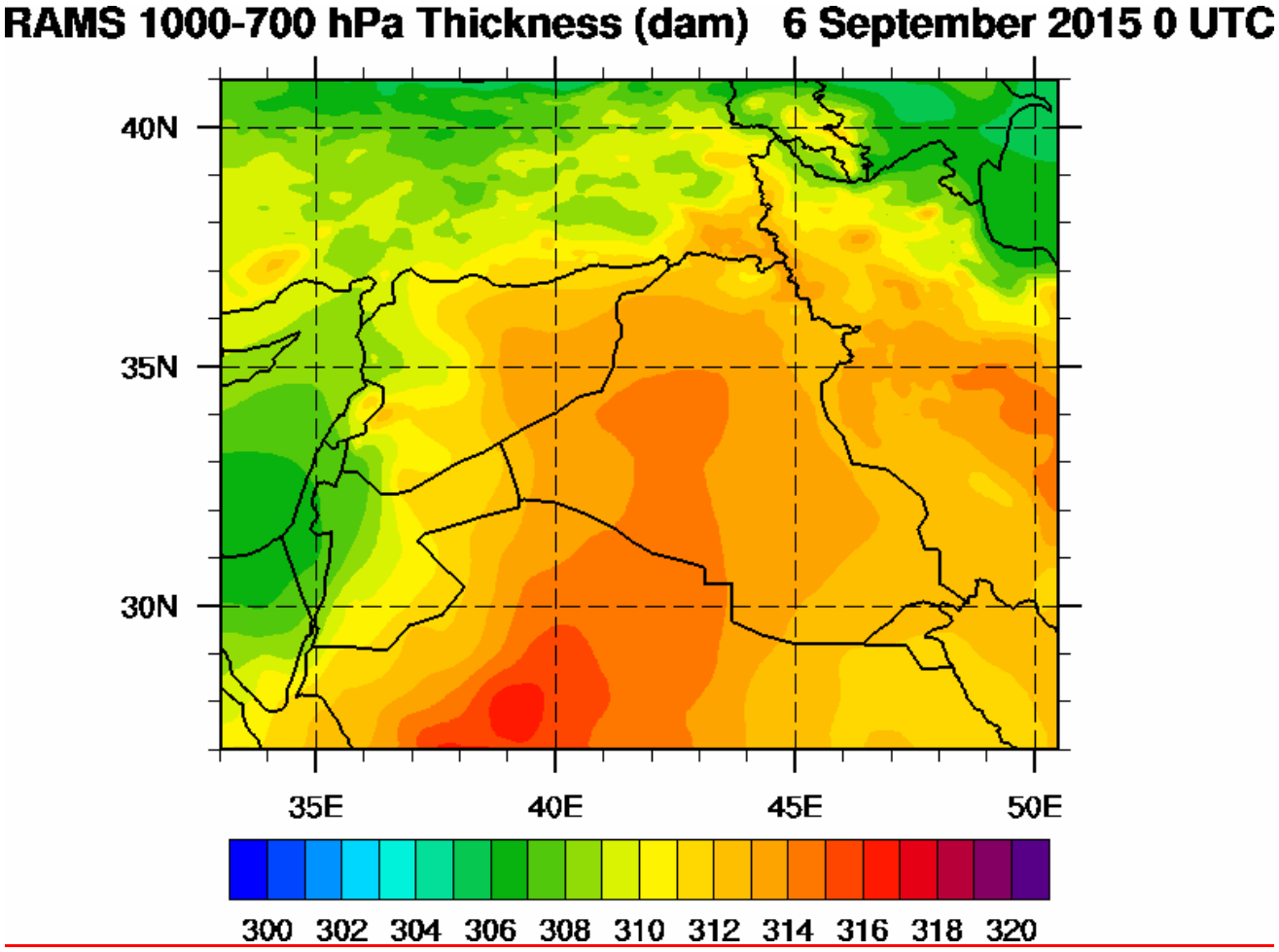
RAMS 1000-700 hPa Thickness (dam) 6 September 2015 0 UTC
40N
35N
30N
35E
40E
45E
50E
300 302 304 306 308 310 312 314 316 318 320

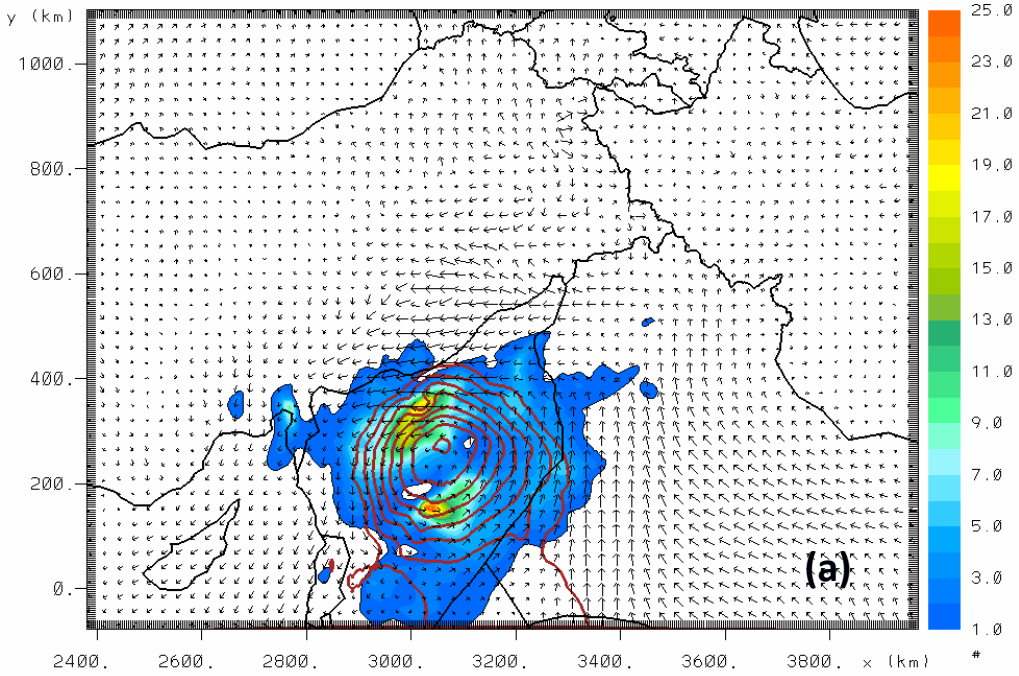
y (km)
1000.
800.
600.
400.
200.
0.
2400.
2600.
2800.
3000.
3200.
3400.
3600.
3800.
x (km)
25.0
23.0
21.0
19.0
17.0
15.0
13.0
11.0
9.0
7.0
5.0
3.0
1.0
(a)

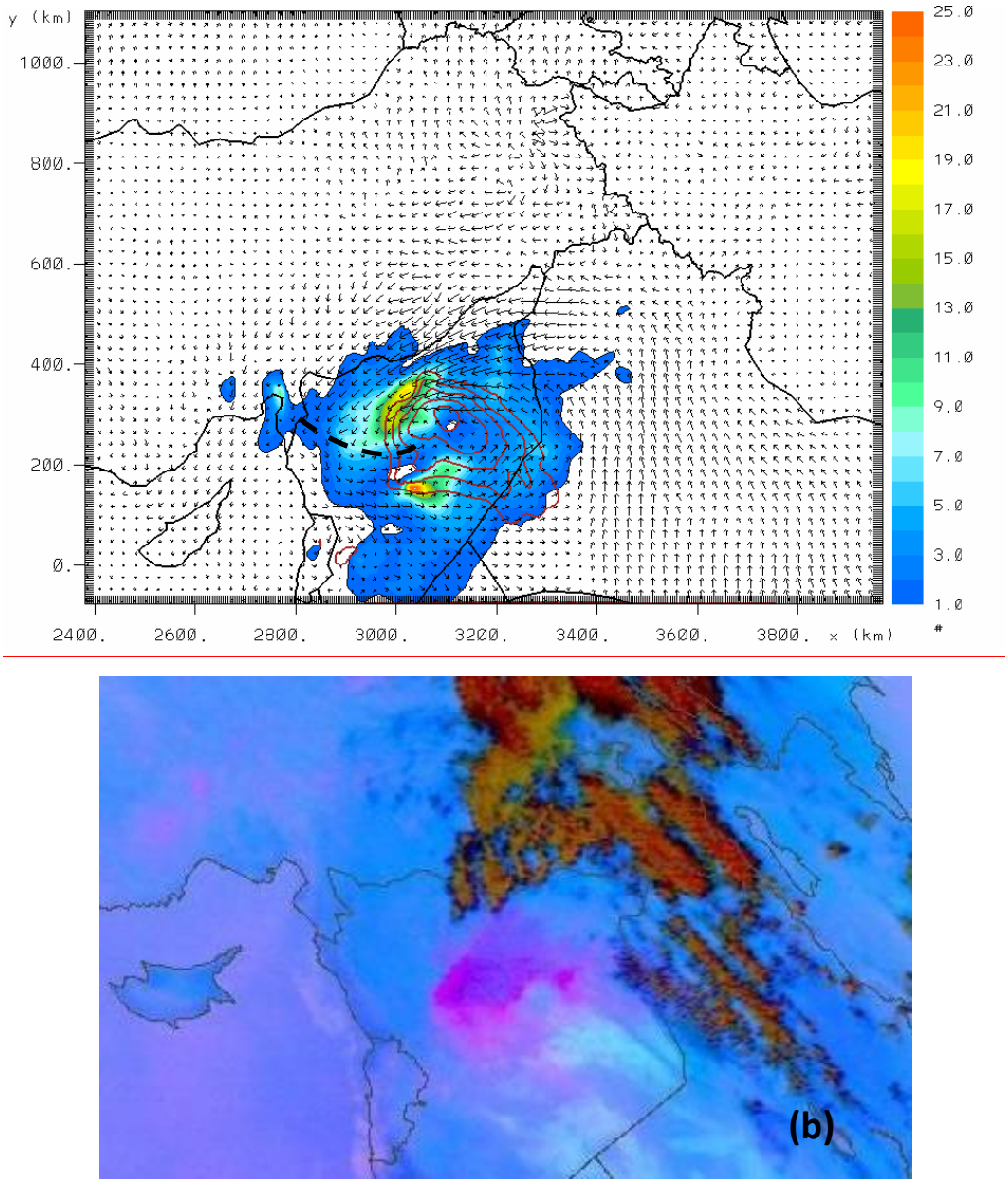

Figure ~~3~~4. a) Model 1000-700 mb thickness (dam), 6 September 2015, 00:00 UTC. Model ~~AOD~~ AOT (color scale) , geopotential height at 850 mb (red contours from 1490 to 1505 m every 2.5 m) and wind vectors at 850mb ; b) MSG SEVIRI dust RGB at 08:00 UTC, 6 September 2015

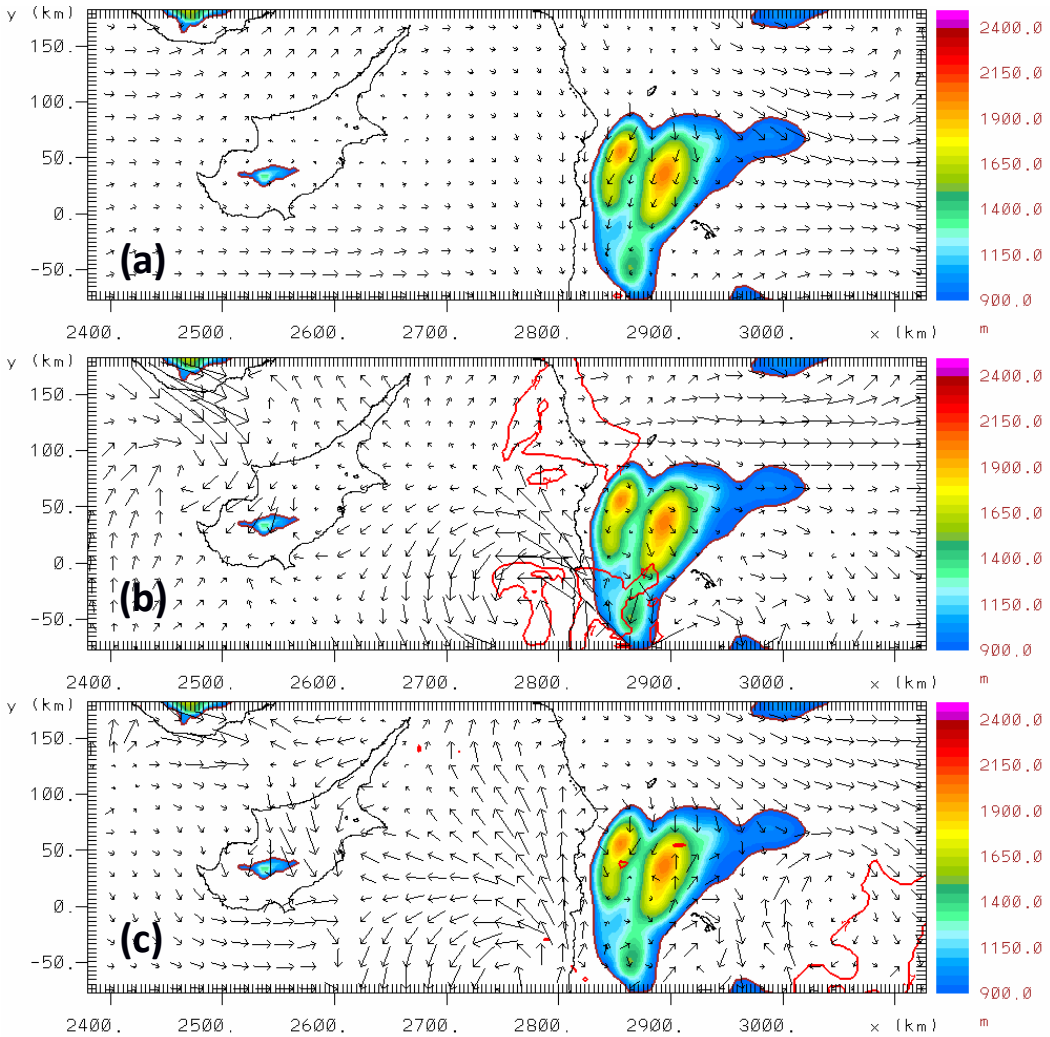

~~Figure 4. Model topography (color scale), wind vectors at the first model layer (50 m) and cloud fraction > 70% (red contour), zoom from the second model grid, 6 September 2015, 00:00, 06:00, 12:00 UTC.~~

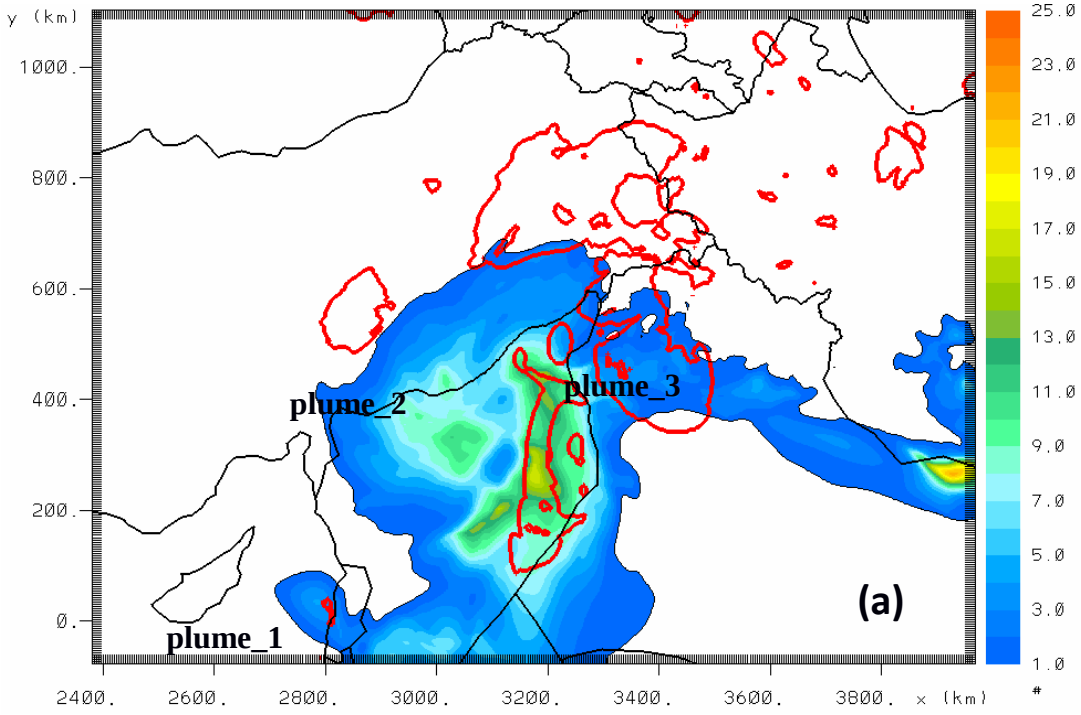

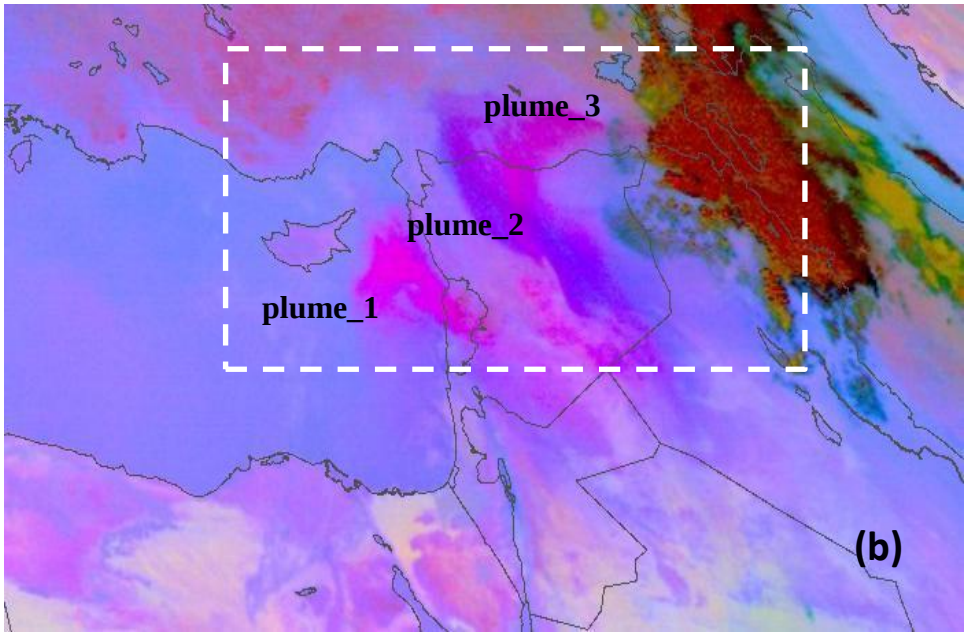

Figure 5. a) Model ~~AOD~~ AOT at 550 nm (color scale) and cloud cover > 70% (red contour). b) MSG-SEVIRI dust RGB component, 7 September 2015, 00:00 UTC. The white rectangular approximately indicates the location of the model domain shown in Figure 5a.

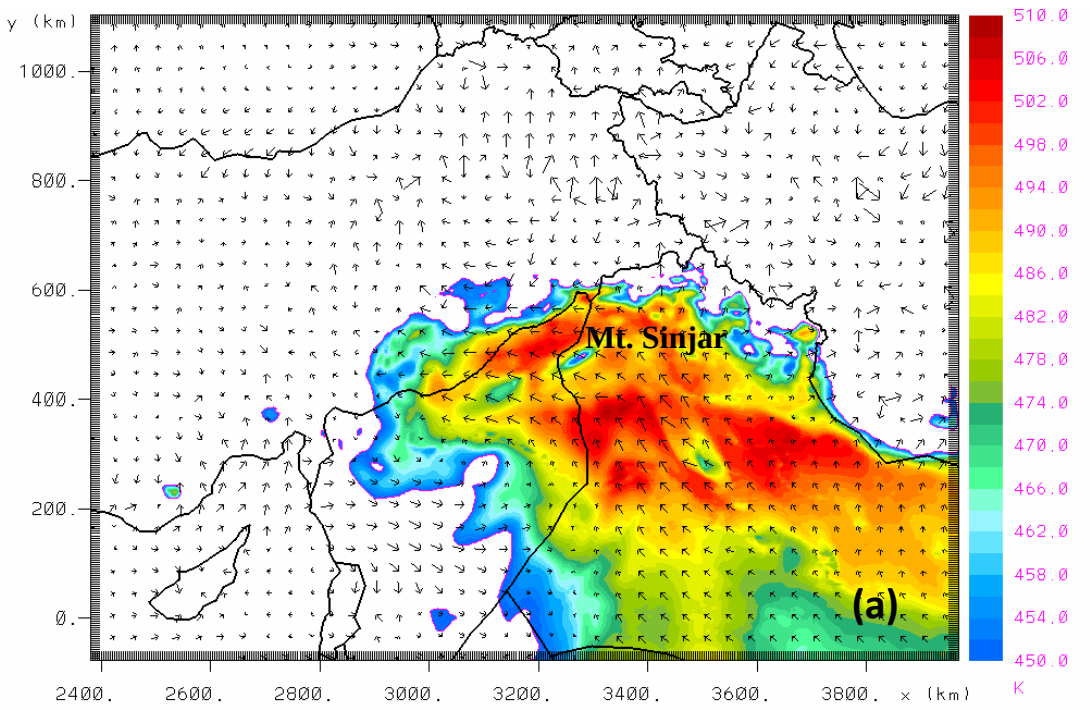
y (km)
1000.
800.
600.
400.
200.
0.
2400.
2600.
2800.
3000.
3200.
3400.
3600.
3800.
x (km)
Mt. Sinjar
(a)
510.0
506.0
502.0
498.0
494.0
490.0
486.0
482.0
478.0
474.0
470.0
466.0
462.0
458.0
454.0
450.0
K

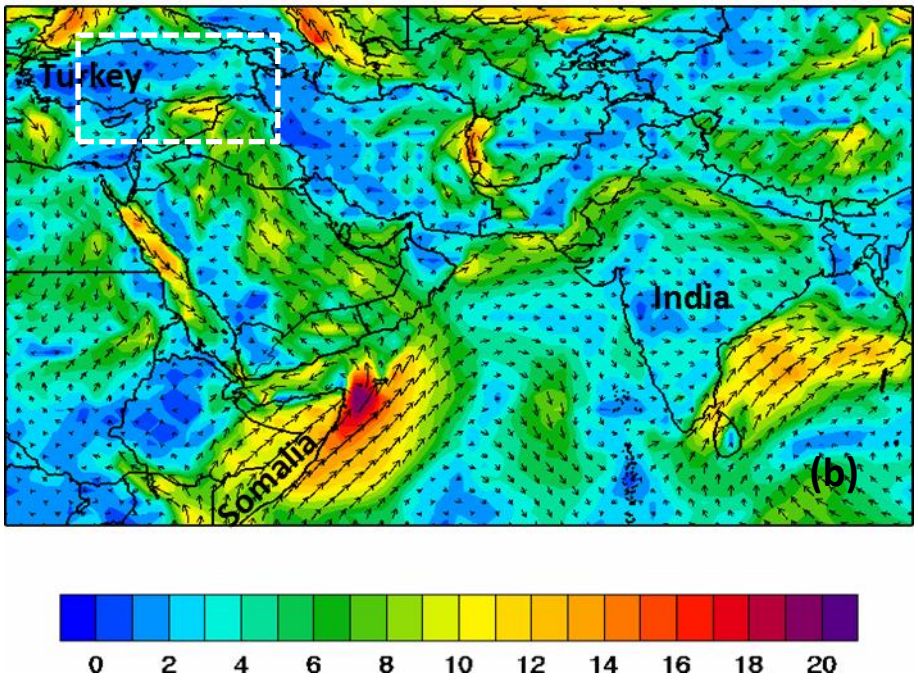
Turkey
India
Somalia
(b)
0
2
4
6
8
10
12
14
16
18
20

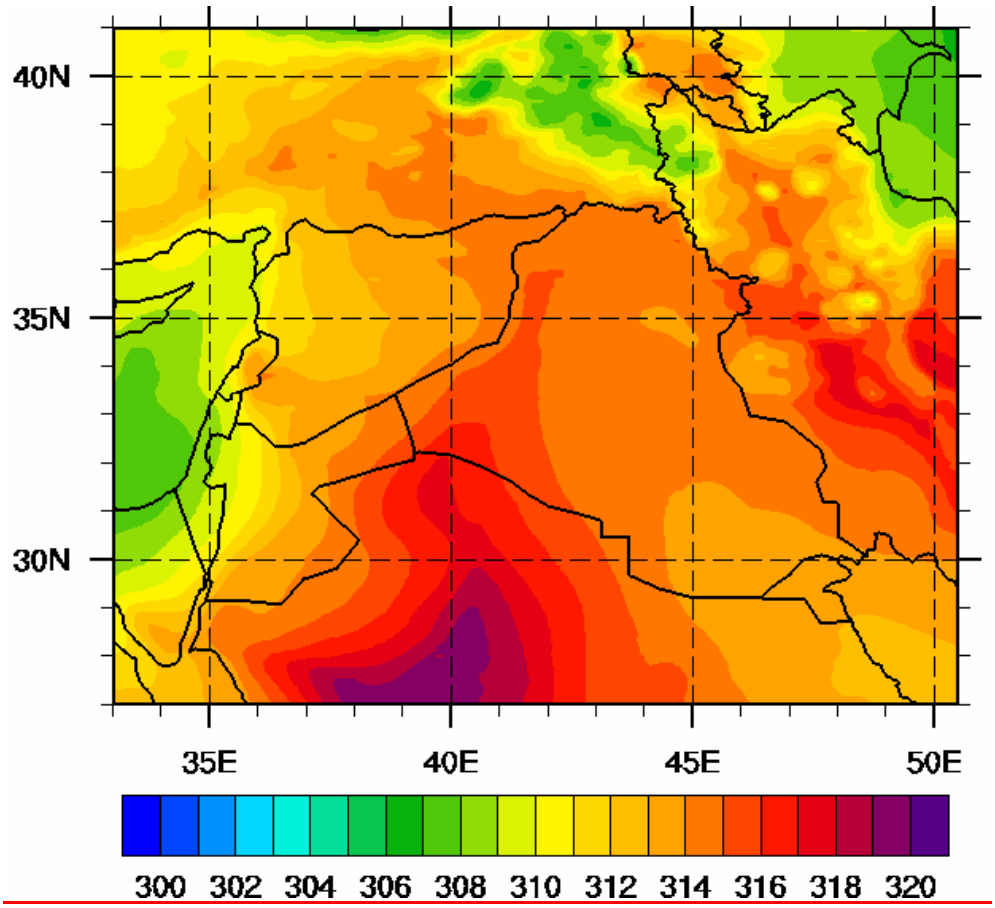

Figure 6. a) Model equivalent potential temperature (K) and wind vectors at 50m above ground, 6 September 2015, 13:00 UTC. b) Wind speed at ~~10m~~ 975 mb from the NCEP final analysis (FNL) dataset, 6 September 2015, 06:00 UTC. The white rectangular indicates the location of the model domain shown in Figure 6a. c) Model 1000-700 mb thickness (dam), 6 September 2015, 15:00 UTC

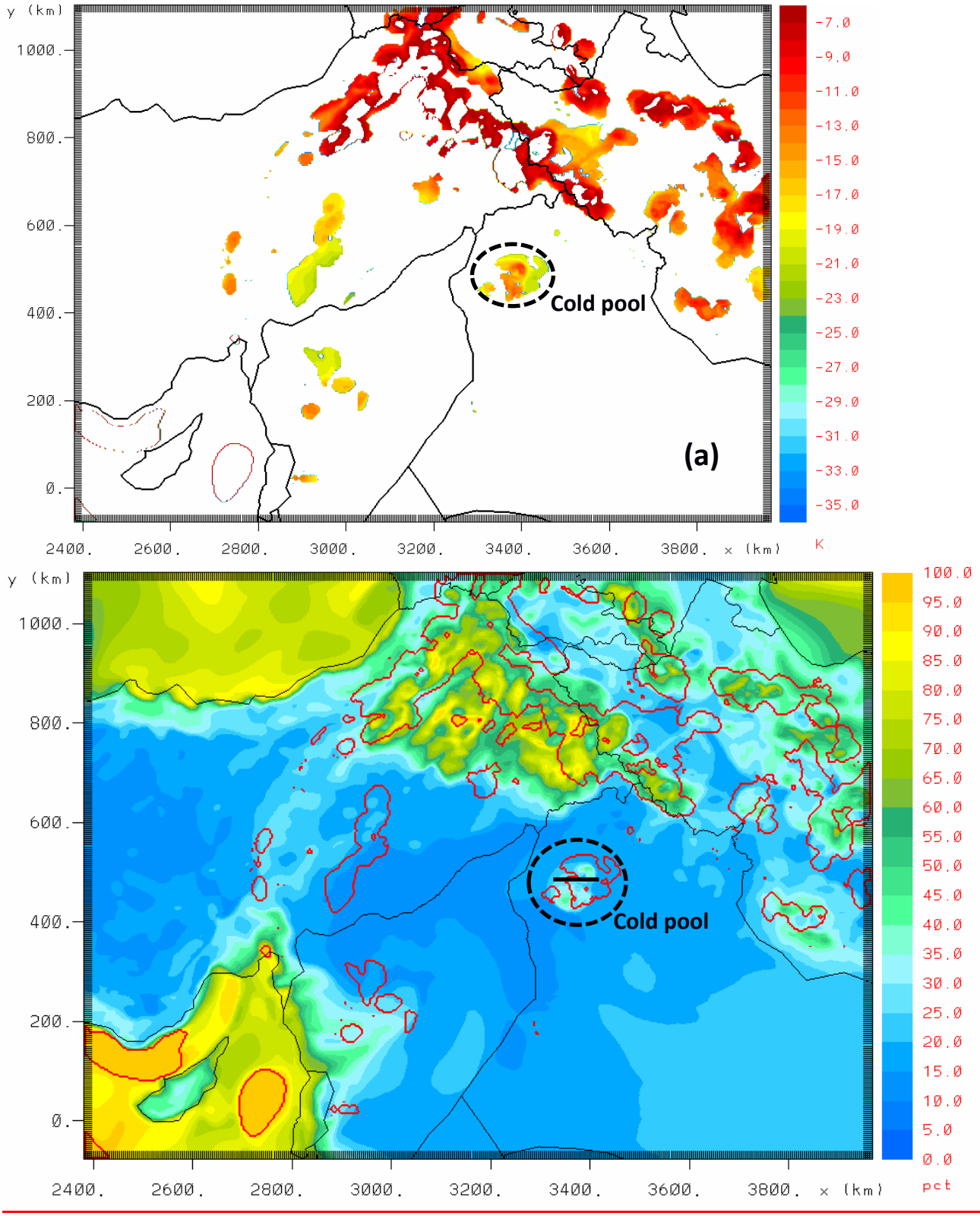
y (km)
1000.
800.
600.
400.
200.
0.
2400.
2600.
2800.
3000.
3200.
3400.
3600.
3800.
x (km)
-7.0
-9.0
-11.0
-13.0
-15.0
-17.0
-19.0
-21.0
-23.0
-25.0
-27.0
-29.0
-31.0
-33.0
-35.0
K
Cold pool
(a)
100.0
95.0
90.0
85.0
80.0
75.0
70.0
65.0
60.0
55.0
50.0
45.0
40.0
35.0
30.0
25.0
20.0
15.0
10.0
5.0
0.0
pct
Cold pool

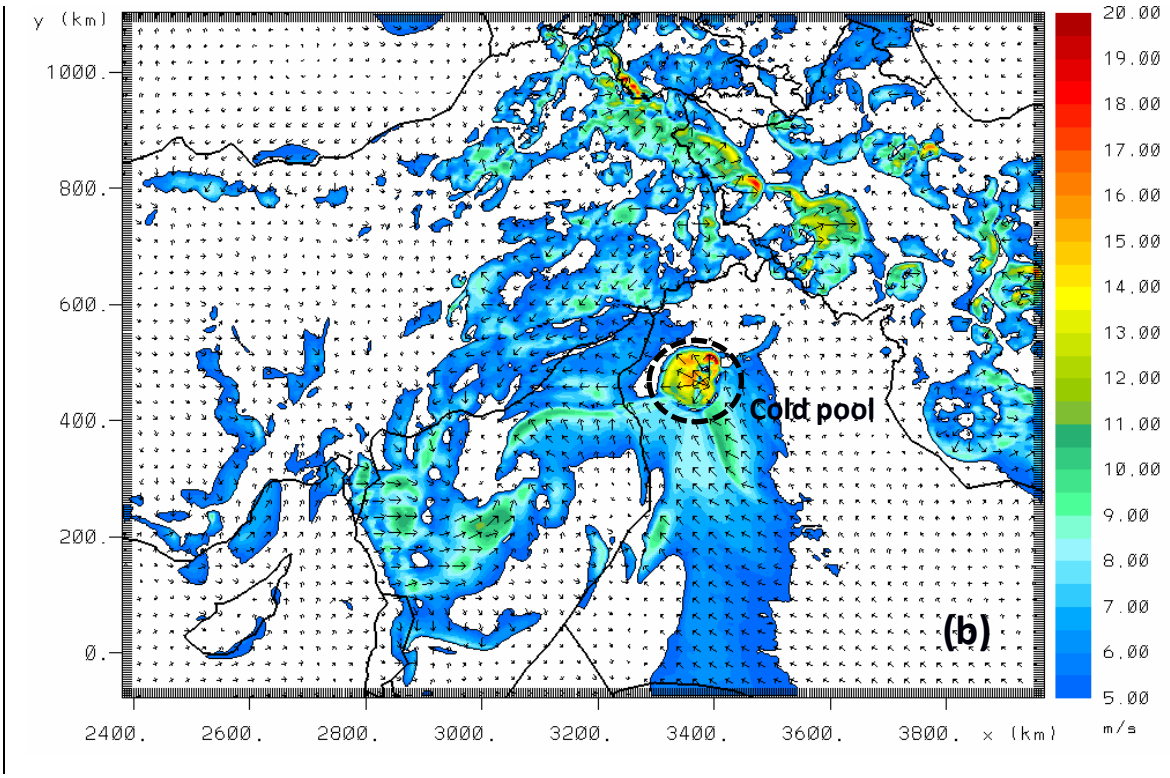
y (km)
1000.
800.
600.
400.
200.
0.
2400.
2600.
2800.
3000.
3200.
3400.
3600.
3800.
x (km)
Cold pool
(b)
20.00
19.00
18.00
17.00
16.00
15.00
14.00
13.00
12.00
11.00
10.00
9.00
8.00
7.00
6.00
5.00
m/s

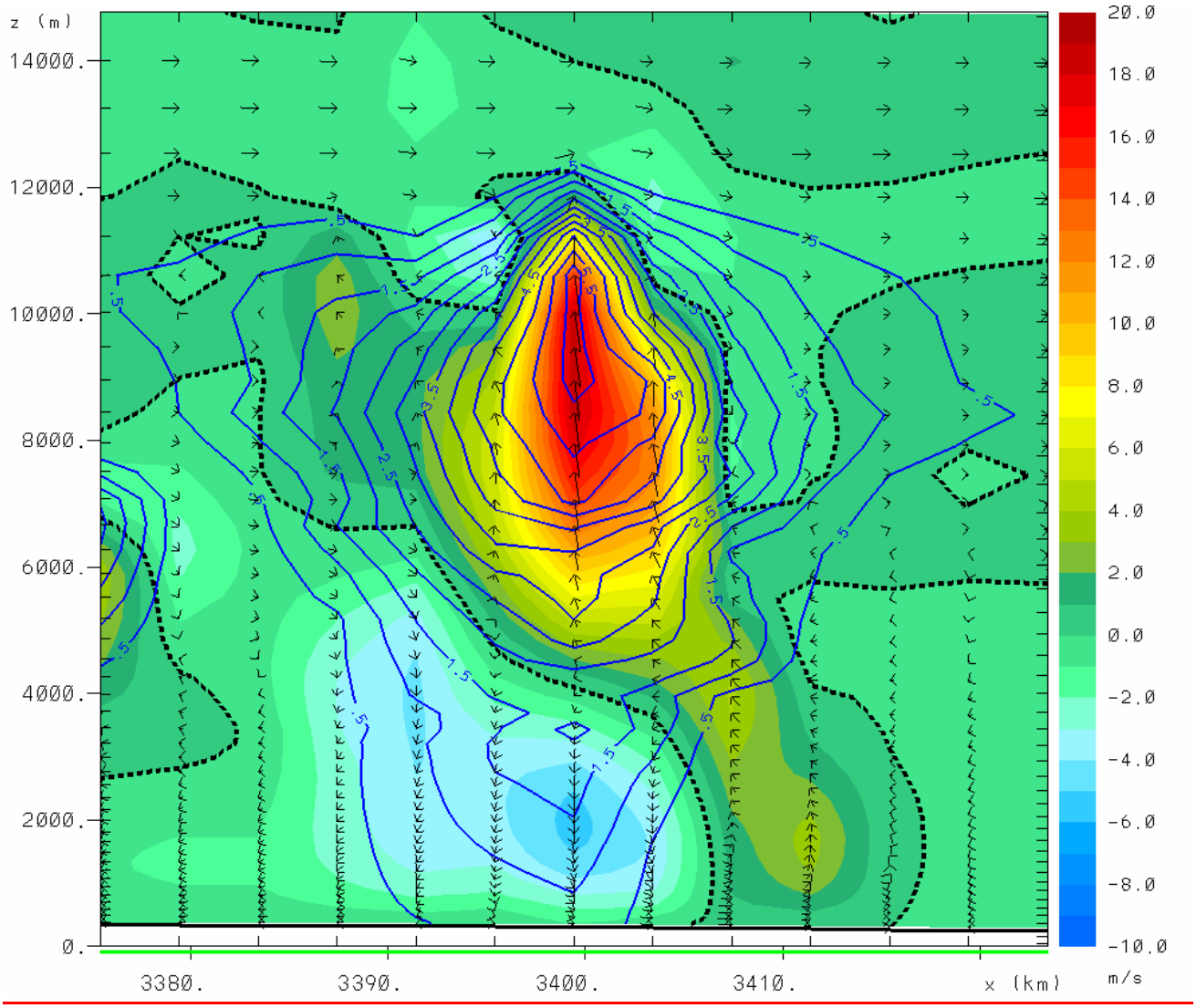
z (m)
14000.
12000.
10000.
8000.
6000.
4000.
2000.
0.
3380.
3390.
3400.
3410.
x (km)
20.0
18.0
16.0
14.0
12.0
10.0
8.0
6.0
4.0
2.0
0.0
-2.0
-4.0
-6.0
-8.0
-10.0
m/s

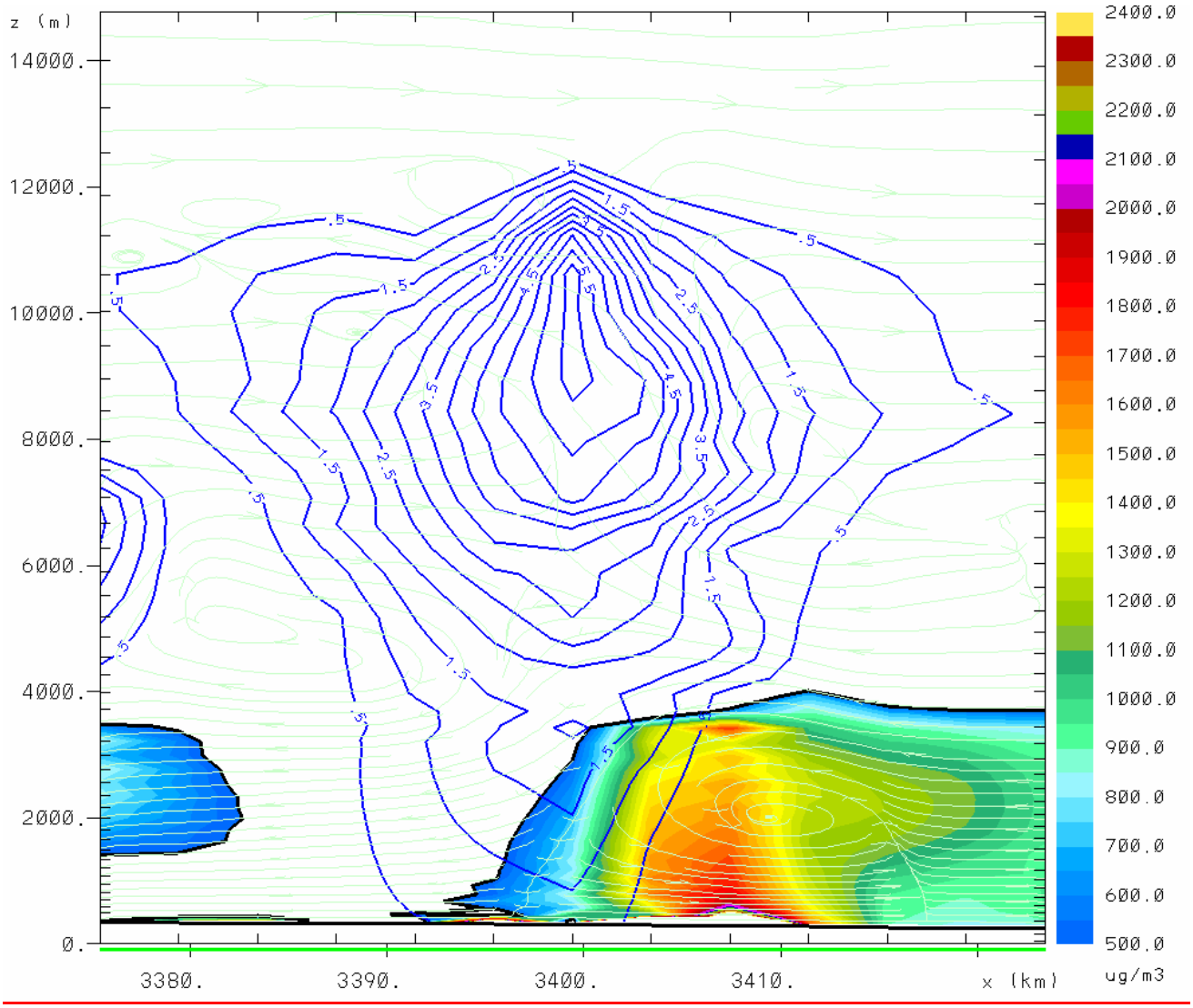

Figure 7. a) Model relative humidity at the first model level (color scale) and -20°C iso-temperature line (red contours) of rain droplets ~~—~~air temperature difference ~~in K~~. b) Model wind speed at 10m (ms^{-1})~~, 6 September 2015, 15:00 UTC~~. The dashed line denotes the location of the cold pool and the solid black line the location of the storm cross-sections of Figures 7c,d~~.~~ c) Vertical cross section of total condensate mixing ratio (blue contours in g k g^{-1}) and vertical wind component (vectors and color scale in m s^{-1}). The dashed line separates updraft (positive w) from downdraft/precipitating regions (negative w). d) Vertical cross section of total condensate mixing ratio (blue contours in g k g^{-1}), dust concentration (μg m^{-3}) and flow streamlines, 6 September 2015, 15:00 UTC

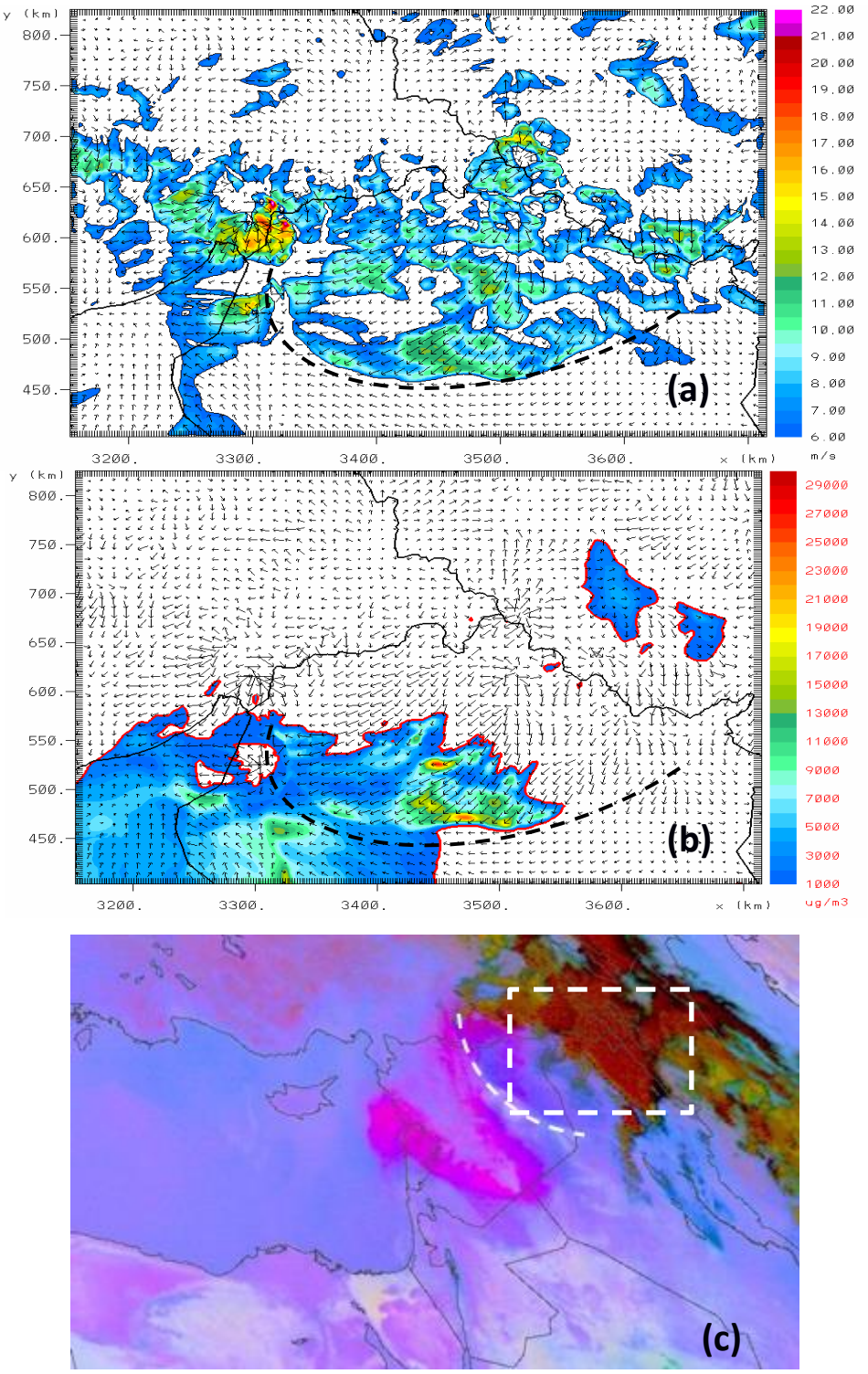

Figure 8. a) Model wind speed greater that 6 ms^{-1} at 10 m and b) Near surface model dust concentration (µg m^{-3}) from the inner grid (2×2km) c) MSG-SEVIRI RGB component, 6 September 2015, 20:00 UTC. The dashed lines indicate the haboob front location and the dashed rectangular in Figure 8c approximately indicates the location of the model domains shown in Figures 8a,b.

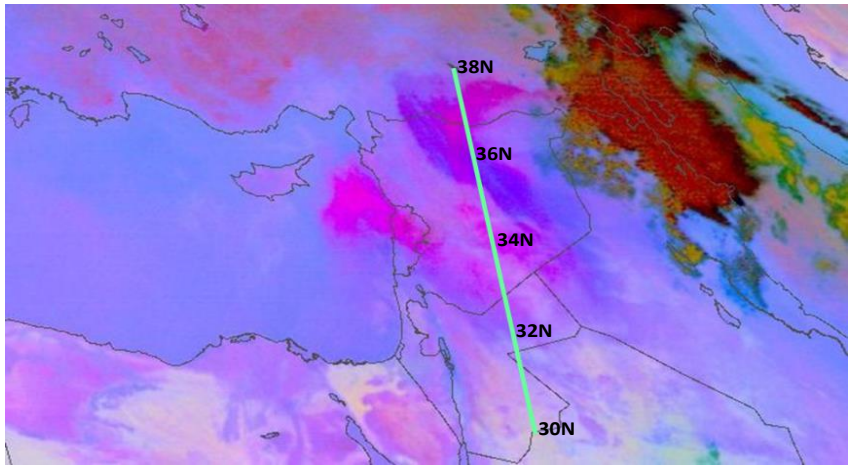
38N
36N
34N
32N
30N

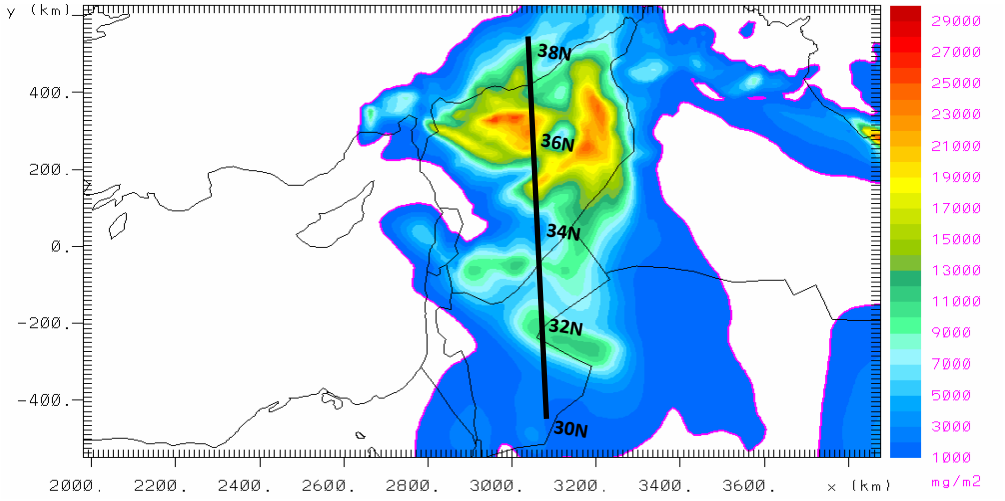
y (km)
400.
200.
0.
-200.
-400.
2000.
2200.
2400.
2600.
2800.
3000.
3200.
3400.
3600.
x (km)
38N
36N
34N
32N
30N
29000
27000
25000
23000
21000
19000
17000
15000
13000
11000
9000
7000
5000
3000
1000
mg/m2

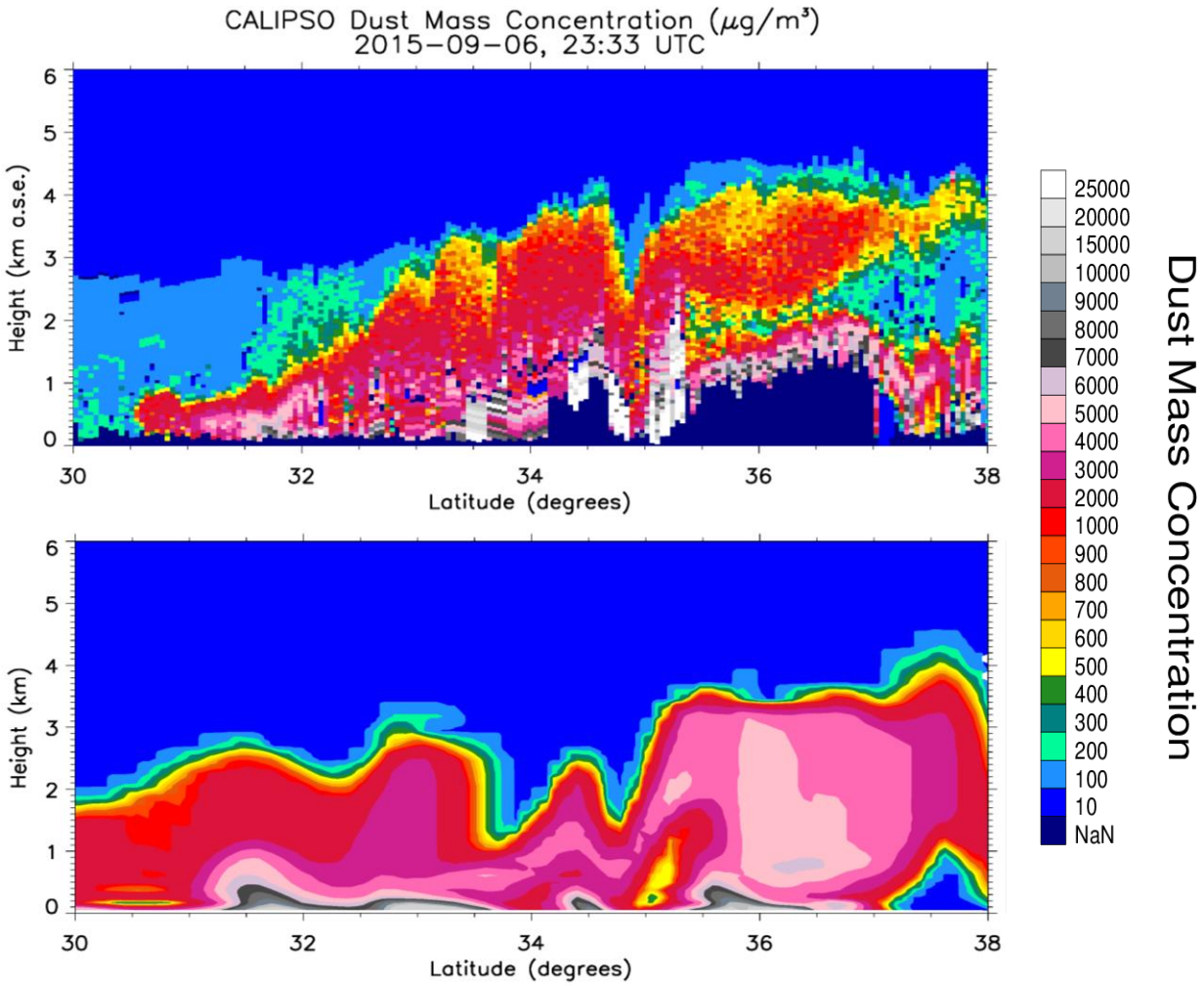

Figure 9. a) MSG-SEVIRI RGB map and CALIPSO overflight (green line), Model dustload (mg m^{-2}) ~~b~~ c) CALIPSO dust mass concentration (μg m^{-3}) and ~~c~~d) model dust mass concentration at 6 September 2015, 23:33 UTC. Due to the severity of the event CALIPSO signal is totally attenuated bellow ~1km a.s.e. in the area between 35-37°N (dark blue color).

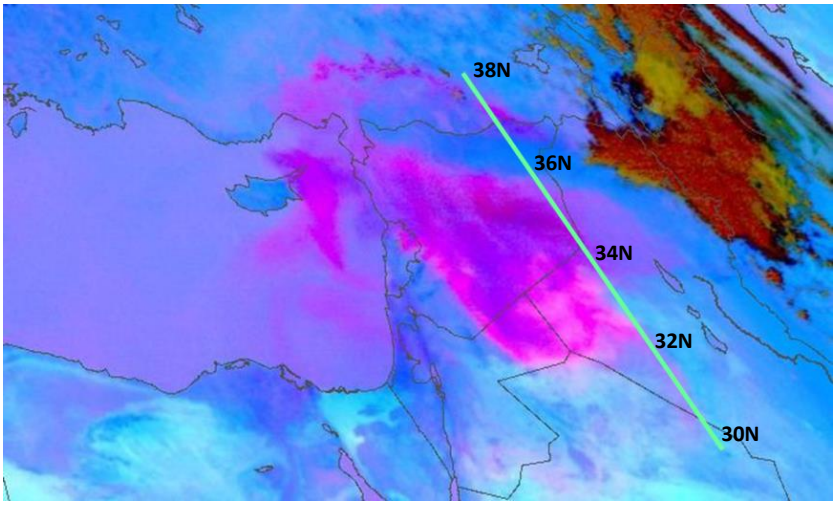
38N
36N
34N
32N
30N

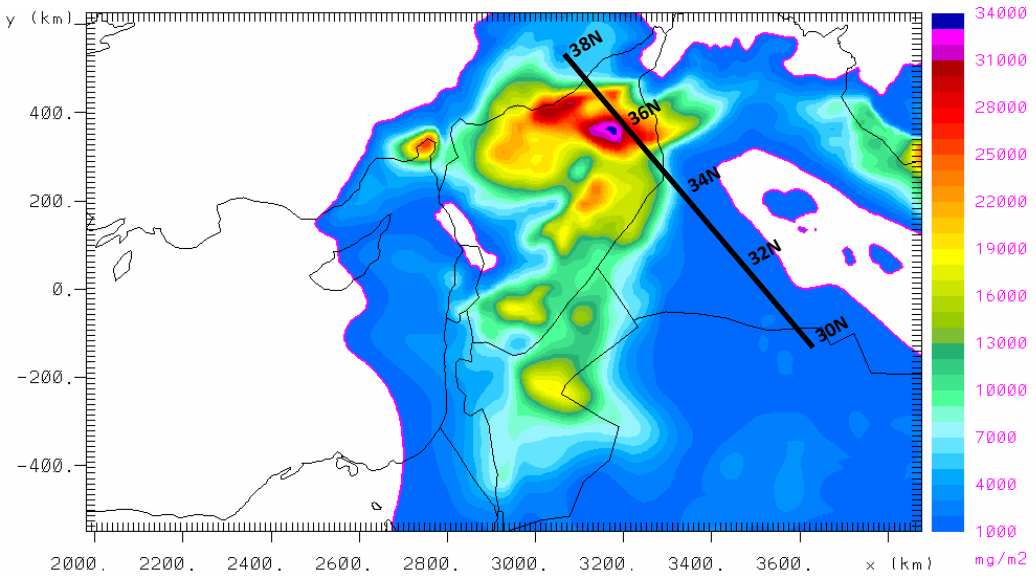
y (km)
400.
200.
0.
-200.
-400.
2000.
2200.
2400.
2600.
2800.
3000.
3200.
3400.
3600.
x (km)
38N
36N
34N
32N
30N
34000
31000
28000
25000
22000
19000
16000
13000
10000
7000
4000
1000
mg/m2

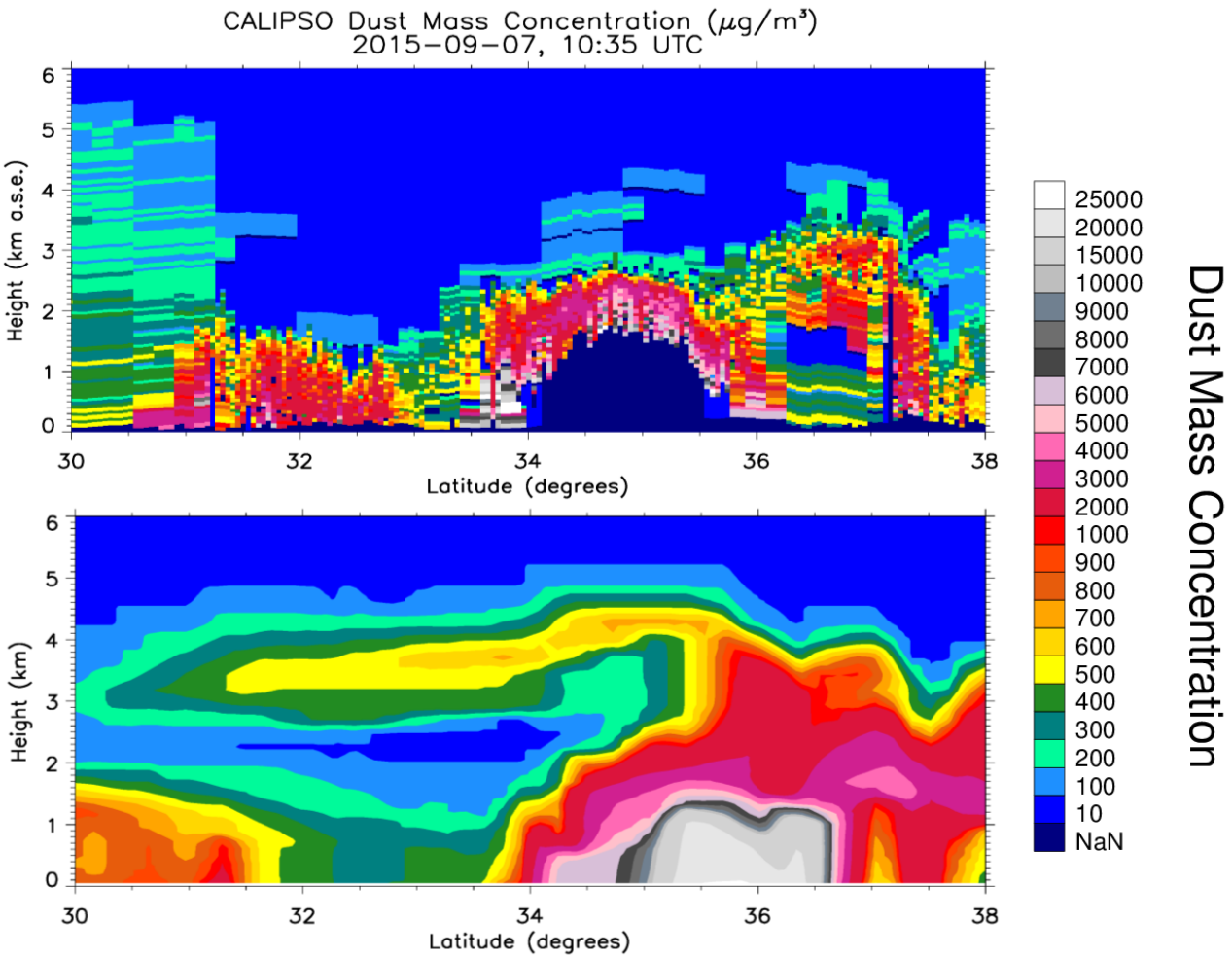

Figure 10. a) MSG-SEVIRI RGB map and CALIPSO overflight (green line), b) Model dustload (mg m^{-2}) c) CALIPSO dust mass concentration (μg m^{-3}) and ~~c~~d) model dust mass concentration at 7 September 2015, 10:35 UTC. Due to the severity of the event CALIPSO signal is totally attenuated bellow ~1km a.s.e. in the area between 34-36°N (dark blue color).

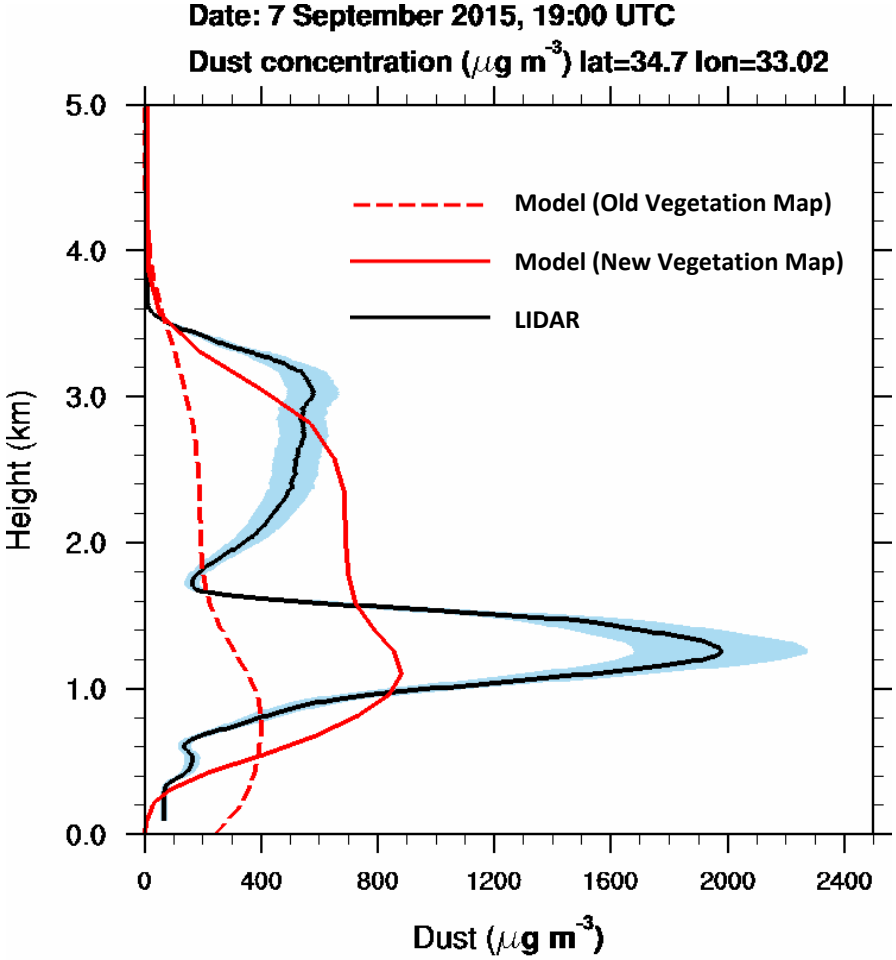

Figure 11. Vertical profile of dust concentration on 7 September 19:00 UTC over Limassol. Blue shadow indicates a 20% uncertainty of the lidar measurements.

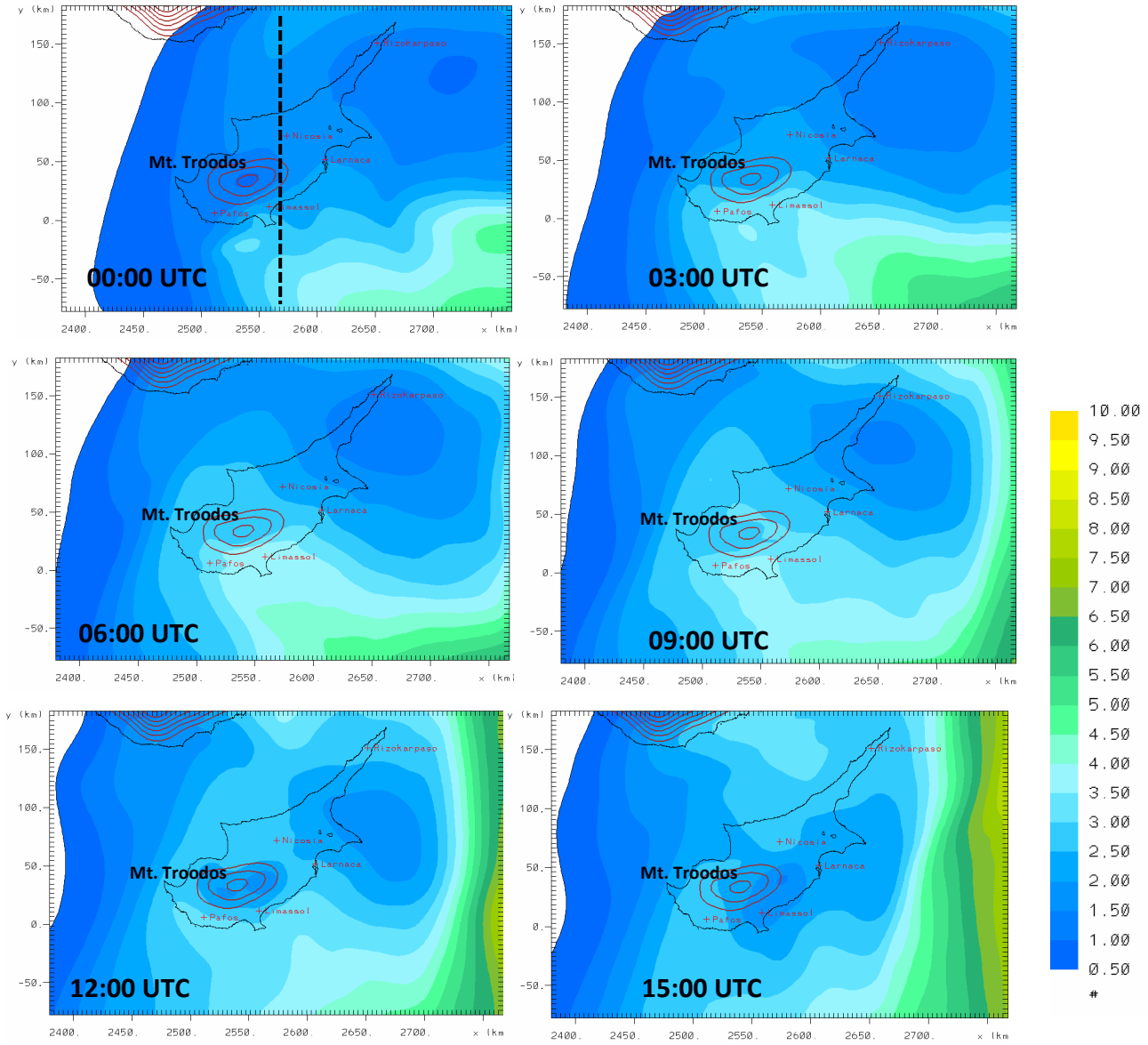

Figure12. Model 550 nm AOT over Cyprus 00:00 – 15:00 UTC, 8 September 2015, zoom from the second (4×4 km) model domain. The dashed black line shows the location of the cross-sections in Figure 13.

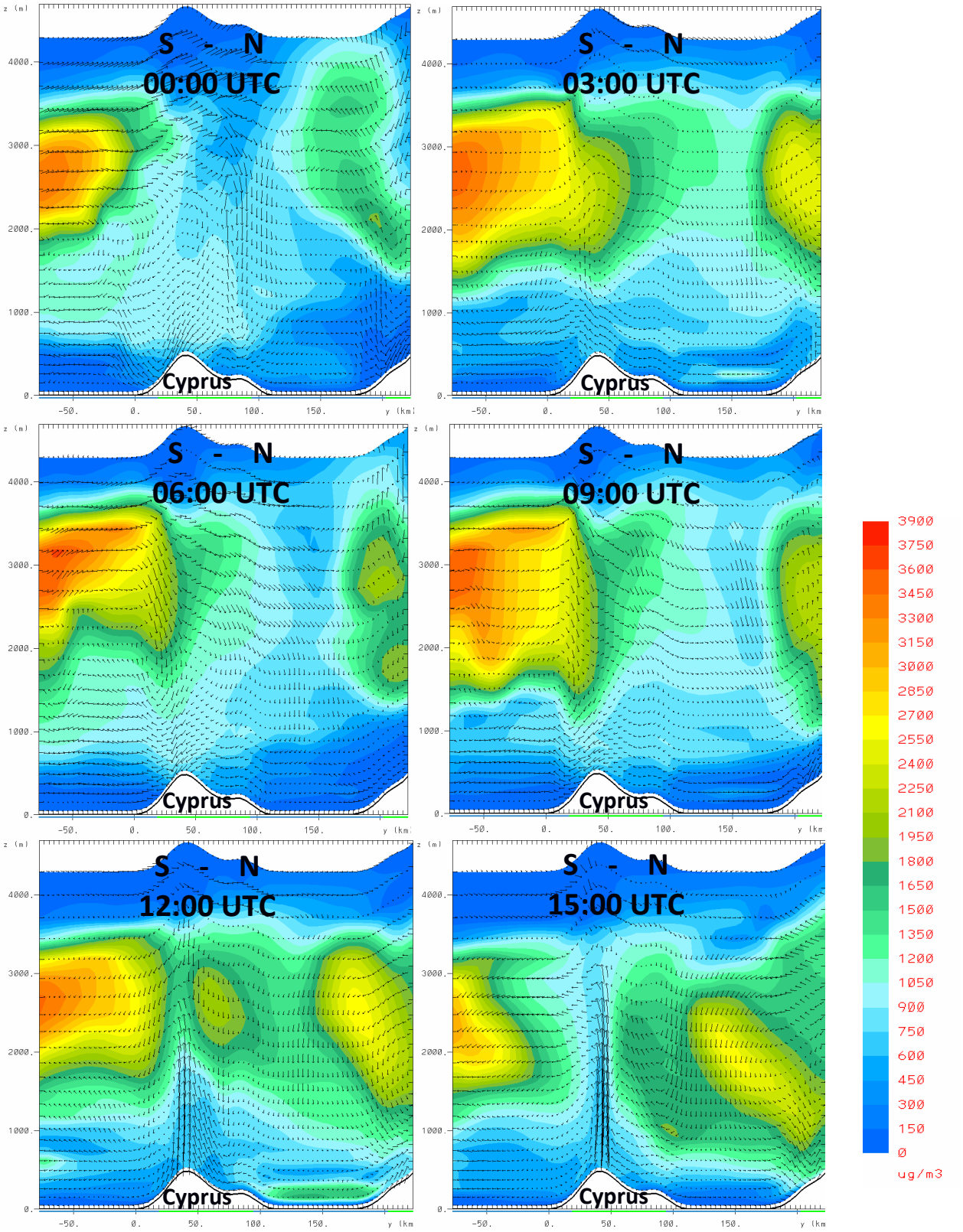

Figure 13. Vertical cross-section (South-North) of modeled dust concentration over Cyprus 00:00 – 15:00 UTC, 8 September 2015. The location of the cross-section is shown in Figure 12a.

Table 1. Range and gamma correction for the Red, Green, and Blue channels for construct the Dust RGB product.

Color	SEVIRI Channels	Min (K)	Max (K)	Γ
Red	IR12.0 – IR10.8	-4	2	1
Green	IR10.8 – IR8.7	0	15	2.5
Blue	IR10.8	261	289	1